Tectonic and magmatic development of the Salinian Coast Ridge Belt, California

Steven Kidder, Mihai Ducea, George Gehrels, P. Jonathan Patchett, and Jeffrey Vervoort

Department of Geosciences, University of Arizona, Tucson, Arizona, USA

Received 6 May 2002; revised 13 May 2003; accepted 9 July 2003; published 24 October 2003.

[1] We present new field, structural, petrographic, and geochronologic data on a rare midcrustal (~25 km) exposure of a Cordilleran arc, the Coast Ridge Belt, located in the Santa Lucia Mountains of central California. The study area is composed primarily of a deformed suite of upper amphibolite to granulite facies rocks (the ''Sur Series''), which is dominated by metaigneous tonalites, diorites, and gabbros with subordinate metasedimentary quartzite and marble. Inherited zircons in magmatic rocks suggest that the provenance of framework rocks is drawn heavily from miogeoclinal formations and that sedimentation occurred in the late Paleozoic or later. Minor magmatism in the Coast Ridge Belt began in the Early or Middle Cretaceous, but magmatic activity was most intense during a short period time from 93 to 81 Ma, based on U-Pb zircon ages of a felsic gneiss and two less-deformed diorites. The time period 93–81 Ma also brackets a period of extensive thickening and high-temperature ductile deformation. While a thrusting cause for ductile deformation cannot be ruled out, we favor the hypothesis that the exposed rocks correspond to a zone of return flow of supracrustal rocks locally displaced by granitoid plutons in the shallower crust. Magmatism ended throughout Salinia between 81 and 76 Ma, coincident with the attainment of peak pressure and temperature conditions of 0.75 GPa and 800°C. Exhumation followed immediately, bringing the Coast Ridge Belt to the surface within 8 My at a rate of at least 2–3 mm/yr. Exhumation was coincident with an episode of extensional collapse that has been documented elsewhere in the southern California arc during the early Laramide orogeny and that may be related to underthrusting of the forearc at that time. *INDEX TERMS:* 8102 Tectonophysics: Continental contractional orogenic belts; 8035 Structural Geology: Pluton emplacement; 3640 Mineralogy and Petrology: Igneous petrology; 8030 Structural Geology: Microstructures; 8124 Tectonophysics: Earth's interior—composition and state (1212); *KEYWORDS:* Salinia, Salinian block, Santa Lucia Mountains, deep arc exposures, amphibolite-granulite, Coast Ridge Belt. **Citation:** Kidder, S., M. Ducea, G. Gehrels, P. J. Patchett, and J. Vervoort, Tectonic and magmatic development of the Salinian Coast Ridge Belt, California, *Tectonics*, *22*(5), 1058, doi:10.1029/2002TC001409, 2003.

0278-7407/03/2002TC001409$12.00

1. Introduction

[2] Cordilleran batholiths are extensive belts of intermediate calc-alkalic plutons formed in the continental crust above subduction zones. Understanding the petrology and tectonic framework of these granitic batholiths has stirred great geologic controversies and continues to pose several major problems in modern geology such as quantifying the rates and processes of crustal growth *versus* recycling in arc environments [e.g., *Hamilton*, 1988]. The key questions are centered around understanding the mechanisms by which continental magmatic arcs may contribute to the production of on average andesitic continental crust, while melt additions from the mantle are basaltic [*Rudnick*, 1995]. Determination of the composition of the crust and upper mantle beneath arcs can provide first-order constraints on defining the processes of magmatic addition and batholith formation and help resolve the crustal compositional paradox.

[3] One of the major limitations in deciphering large-scale magmatic and deformational features in arcs is a poor knowledge of their vertical dimension. Most major active or recent continental arcs are located around the Pacific, the largest ones being found along the western margins of North and South America. Exposures of arcs to paleodepths in excess of 20 km are virtually absent in South America, and rare in the North American Cordillera. North American exposures are not deeper than some 30 km, although seismic [*Graeber and Asch*, 1999] and xenolith [*Ducea and Saleeby*, 1996] data suggest that Cordilleran arc crustal thickness is commonly about 75 km. With very limited arc-related middle or deep-crustal exposures available around the Pacific Rim, seismic velocity has been used with various degrees of success to estimate crustal composition [*Smithson et al.*, 1981; *Christensen and Mooney*, 1995; *Rudnick and Fountain*, 1995]. Much less is known about the interplay between deformation and magmatism at middle to deep-crustal levels in arcs [*Paterson and Miller*, 1998]. One of the most important issues in studies of convergent margins is the question of the degree to which crustal thickening at continental arcs is ''magmatic'' versus ''tectonic''. Magmatic thickening refers to addition of melts from the Earth's mantle during the buildup of the arc, whereas tectonic thickening requires crustal shortening, intracrustal deformation, and crustal melting to be major process in continental arc

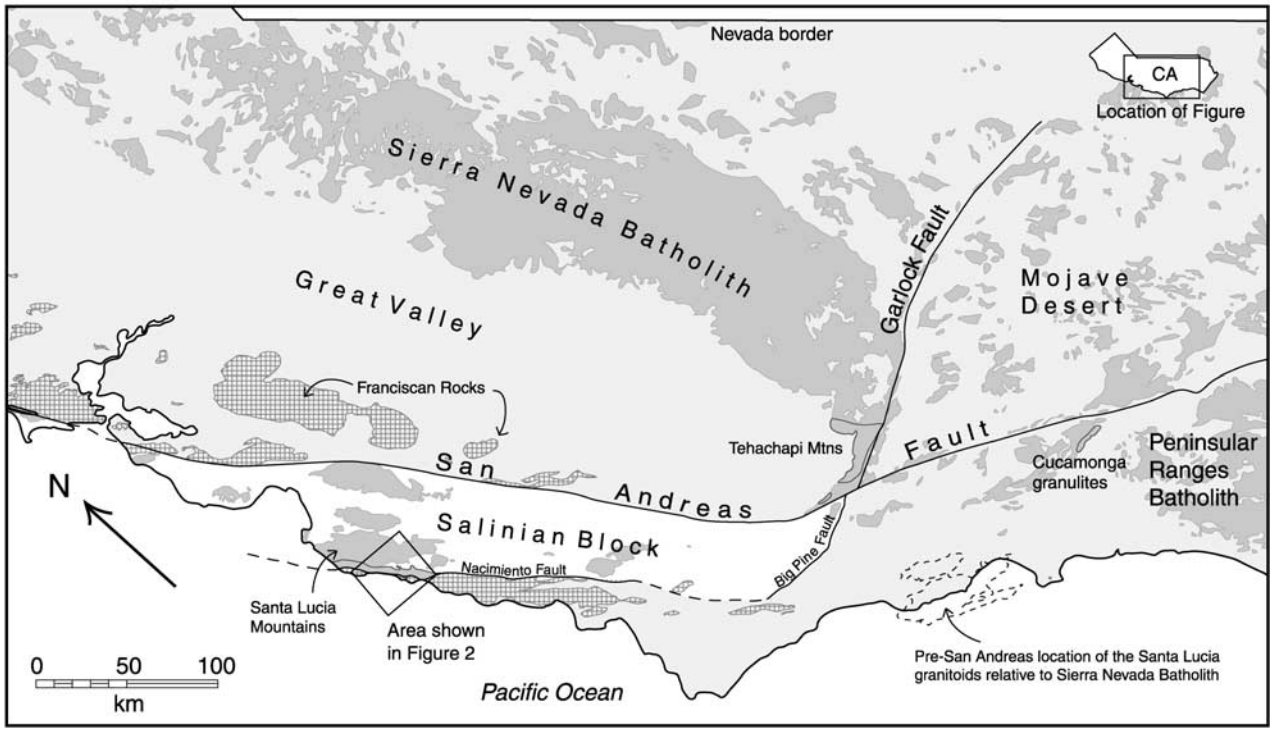

Figure 1. Map of central and southern California showing geologic features discussed in the text. Mesozoic granitic and related metamorphic rocks are shaded lightly. Fine-gridded areas are mainly Jurassic Franciscan formation. Mesozoic amphibolite-granulite terranes are outlined and labeled. The restored location of the Santa Lucia Mountains is based on palinspastic reconstruction prior to disruption by the San Andreas Fault system (~20 Ma; *Powell* [1993]). Restoration is relative to the southern Sierra Nevada.

environments. Are the well-established magmatic flare ups in major continental arcs largely determined by episodes of crustal shortening [e.g., *Ducea*, 2001], or are they predominantly driven by fluctuations of melt productivity in the mantle wedge?

[4] We address the above questions regarding the composition and evolution of arc crust with new geologic results from a midcrustal exposure of the Cretaceous continental arc located in the Santa Lucia Mountains. The Santa Lucia Mountains are located in the California Coast Ranges and comprise predominantly upper crustal, Mesozoic, out of place arc-related rocks of the allochthonous Salinian terrane (Figure 1). Rocks exposed however in the Coast Ridge Belt, a narrow zone along the southwestern edge of the Santa Lucia mountains, were significantly deeper based on the presence of upper amphibolite and granulite facies rocks [*Compton*, 1966b; *Hansen and Stuk*, 1993]. We present here a detailed map of a transect across the Coast Ridge Belt, a geologic and petrographic description of the metamorphic framework and four previously undocumented intrusions, and U/Pb and Sm/Nd data constraining ages of deformation, intrusion, metamorphism and uplift in the Coast Ridge Belt. Specifically, we address the following questions in this study: (1) the origin of the framework rocks in the area, (2) the timing relationships between deformation and magmatism, (3) the origin of ductile fabrics, (4) the conditions and timing of peak metamorphism in the section and (5) the exhumation history of the arc.

2. Geologic Background

[5] The Salinian block or Salinian ''composite terrane'' [*Vedder et al.*, 1982] is located west of the San Andreas fault, east of the Sur and Nacimiento faults, and north of the Big Pine fault (Figure 1). On the basis of the ages and isotopic characteristics of widespread calc-alkaline to calcic tonalites and granodiorites characterized by *Ross* [1978], *Mattinson* [1990] suggested an origin for the Salinian basement as a middle to lower crustal exposure of a west facing Cretaceous arc straddling the cratonic margin. Magmatic activity in the Salinian arc most likely began between 100 and 110 Ma, and continued until 76 Ma [*Mattinson*, 1990], coincident with the major pulse of magmatism that generated the main segments of the California arc, the Sierra Nevada and Peninsular Ranges batholiths [*Ducea*, 2001; *Coleman and Glazner*, 1998].

[6] Heterogeneous gneisses and schists found in the Santa Lucia Mountains and elsewhere in the Salinian composite terrane are known collectively as the ''Sur Series'' [*Trask*, 1926]. The Sur Series forms the metamorphic framework for most of the Cretaceous intrusions and is composed predominantly of quartzofeldspathic gneiss and granofels, quartz biotite schists, marbles and amphibolites

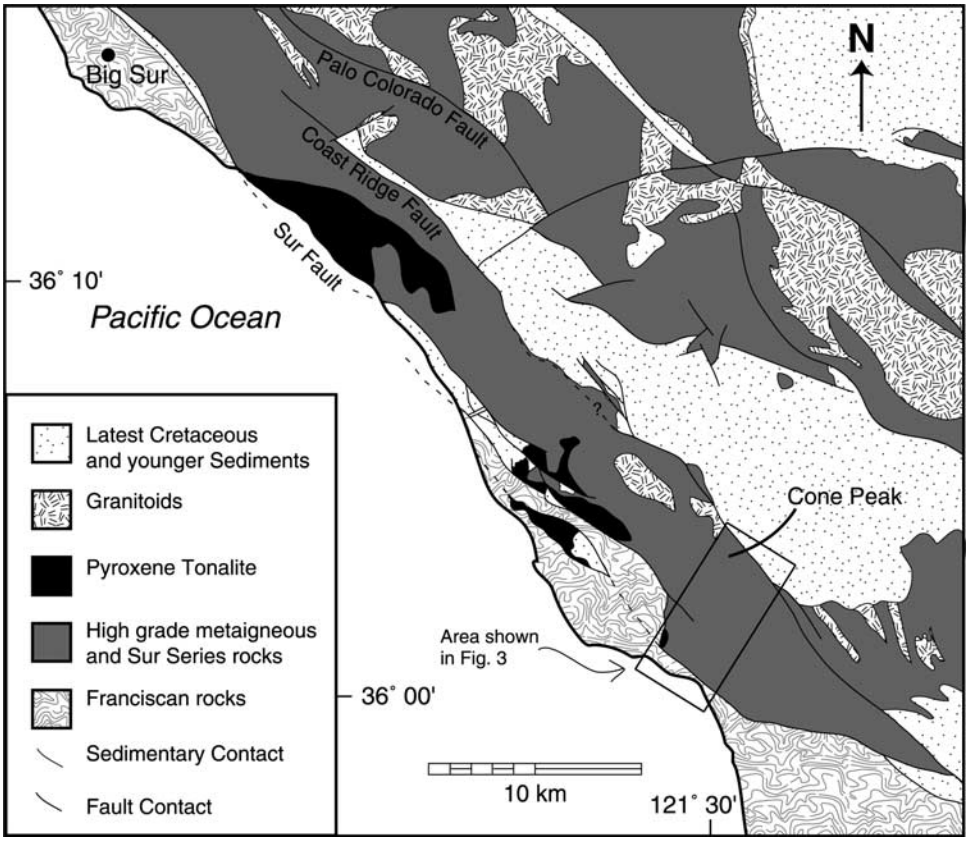

Figure 2. Geologic map showing a portion of the Salinian composite terrane near Big Sur, California. The Coast Ridge Belt is bounded by the Coast Ridge fault to the east and by Franciscan rocks on the west. Figure 2 is based on *Seiders et al.* [1983] and *Ross* [1976]. See Figure 1 for its location. Courtesy of the U.S. Geological Survey.

[*Ross*, 1977]. These lithologies have been interpreted to represent metamorphosed medium to fine-grained clastic sedimentary material [*Ross*, 1977] deposited perhaps as a ''shallow, platformal sequence of continental margin origin'' [*Mattinson*, 1990]. Folding and metamorphism related to numerous intrusions have thoroughly obscured the original sedimentary sequence or sequences, and have prohibited descriptions of stratigraphy and estimations of sedimentary ages [*Wiebe*, 1970a; *Ross*, 1977; *James and Mattinson*, 1988]. Although it has no *stratigraphic* meaning, the term Sur Series has remained in use.

[7] The Salinian rocks are currently juxtaposed to the west and east against the Mesozoic accretion-related Franciscan assemblage and are thus tectonically ''out of place'' (Figure 1). There is little argument that the Salinian composite terrane has traveled northward some 330 km during the Late Cenozoic along the San Andreas fault system (Figure 1; *Powell* [1993]), and petrologic, isotopic, structural and sedimentologic evidence have placed it near the southern end of the Sierra Nevada Batholith during the Cretaceous as well [*Hill and Dibblee*, 1953; *Page*, 1981; *Dickinson*, 1983; *Ross*, 1984; *Silver and Mattinson*, 1986; *Hall*, 1991; *Grove*, 1993; *Schott and Johnson*, 1998]. This hypothesis has been questioned based on paleomagnetic evidence for right-lateral offset of Salinian sedimentary and granitic rocks by thousands of km relative to the North American Cordillera [e.g., *Champion et al.*, 1984; *Kanter and Debiche*, 1985]. However, recent paleomagnetic data [*Dickinson and Butler*, 1998] strongly argue against the large transport hypothesis for Salinia.

[8] While late Cretaceous uplift exposed much of the Salinian arc to shallow or mesozonal depths of up to ~0.4–0.6 GPa [*Wiebe*, 1970a], limited 0.7–0.8 GPa exposures [*Hansen and Stuk*, 1993] surfaced along what is now the western edge of the Santa Lucia Mountains. The current study encompasses a transect of these rocks from the Sur fault to the Cone Peak area (Figure 2). These deeper rocks have been referred to as the Coast Ridge section [*Reich*, 1937], Coast Ridge Belt [*Ross*, 1976] and Salinian Western block [*Ross*, 1978]. *Ross* [1976] linked the Coast Ridge fault with the Palo Colorado fault (Figure 2), thereby severing the deeper ''Salinian Western block'' rocks from the Salinian Central block. In other maps of the area the Coast Ridge fault has not been considered a through-going structure [*Jennings and Strand*, 1959; *Hall*, 1991; L. I. Rosenberg, unpublished data, 2001]. In either case there is little reason to invoke large offsets between the deeper rocks exposed along the Coast Ridge and those in the central part of the Santa Lucia Range. Metamorphic grade increases gradually as the Coast Ridge Belt is approached from the east [*Wiebe*, 1970b; *Compton*,

Table 1. U-Pb Analyses by ID-TIMS[a]

Number of Grains	Weight, μg	U, ppm	Pb, ppm	$^{206}Pb/^{204}Pb$	$^{208}Pb/^{206}Pb$	$^{206}Pb/^{238}Pb$ (Error)	$^{207}Pb/^{235}U$ (Error)	$^{207}Pb/^{206}Pb$ (Error)	Age, Ma		
									$^{206}Pb/^{238}Pb$	$^{207}Pb/^{235}U$	$^{207}Pb/^{206}Pb$
4	86	65	1.2	1041	0.21	0.01706 (1.8)	0.14833 (2.5)	0.06305 (1.7)	109.1	140.4	710
4	72	43	0.7	471	0.15	0.01442 (3.4)	0.09689 (5.6)	0.04873 (4.2)	92.3	93.9	134.8
4	78	132	2.2	456	0.15	0.01467 (1.7)	0.09589 (5)	0.0474 (4.5)	93.9	93	69.6
4	65	111	2.1	701	0.16	0.01683 (1.5)	0.12321 (3.1)	0.0531 (2.6)	107.6	118	333.3
1	21	122	2	369	0.22	0.01445 (4.8)	0.09884 (7.6)	0.04961 (5.6)	92.5	95.7	177
1	26	112	2.1	275	0.17	0.01569 (3.5)	0.11168 (7)	0.05161 (5.9)	100.4	107.5	268.3
1	30	57	1	158	0.13	0.01431 (5.8)	0.09645 (12.4)	0.04889 (10.5)	91.6	93.5	142.4
1	18	91	1.5	209	0.14	0.01449 (6.4)	0.09111 (11.2)	0.0456 (8.9)	92.8	88.5	−23.7

[a]All grains analyzed were highly translucent euhedral crystals, ∼250 μ in length. $^{206}Pb/^{204}Pb$ is the measured ratio, uncorrected for blank, spike, or fractionation. $^{208}Pb/^{206}Pb$ is corrected for blank, spike, and fractionation. Concentrations have an uncertainty of up to 25% due to the uncertainty of weight of grain. Constants used: $\lambda 235 = 9.8485 \times 10^{-10}$; $\lambda 238 = 1.55125 \times 10^{-10}$; $^{238}U/^{235}U = 137.88$. All uncertainties are at the 95% confidence level. Isotope ratios are adjusted as follows: (1) mass-dependent corrections factors of 0.14 ± 0.06%/amu for Pb and 0.04 ± 0.04%/amu for UO2; (2) Pb ratios corrected for 0.005 ± 0.003 ng blank with $^{206}Pb/^{204}Pb = 18.6 \pm 0.3$, $^{207}Pb/^{204}Pb = 15.5 \pm 0.3$, and $^{208}Pb/^{204}Pb = 38.0 \pm 0.8$; (3) U has been adjusted for 0.0005 ± 0.0005 ng blank; (4) initial Pb from *Stacey and Kramers* [1975], with uncertainties of 1.0 for $^{206}Pb/^{204}Pb$, 0.3 for $^{207}Pb/^{204}Pb$, and 2.0 for $^{208}Pb/^{204}Pb$.

1966b], and rocks found on both sides of the fault are similar petrographically [*Compton*, 1966b]. For these reasons we consider the rocks exposed along the Coast Ridge a deeper extension of the Salinian Central block rather than a separate tectonic entity. In this view the basement rocks exposed near Cone Peak and continuing east of the Coast Ridge represent a tilted exposure of a Cordilleran magmatic arc with exposure depths ranging from 25 km in the west to some 10 km in the east.

3. Analytical Techniques

[9] Electron microprobe analysis on minerals were carried out at the University of Arizona using the Cameca SX50 microprobe equipped with 5 LiF, PET and TAP spectrometers. Counting times for each element were 30 s at an accelerating potential of 15 kV and a beam current of 10 nA. Measurements with oxide totals outside of the range 100 ± 1% were discarded with the exception of clinopyroxene in sample 730-4 and clinopyroxene and plagioclase in 710−5 for which sample totals between 98.5% and 99% were also used.

[10] Three samples were processed for U-Pb analyses. Zircons from one sample were analyzed successfully by conventional ID-TIMS using a VG-354 multicollector mass spectrometer using techniques described by *Gehrels* [2000]. The results from ID-TIMS analyses are reported in Table 1 and shown on a conventional concordia diagram (Figure 7). ID-TIMS analyses of the other two samples were not possible due to the very low U concentration (generally <10 ppm U) in most grains and the presence of inherited components. Zircons from these samples were accordingly also analyzed by laser ablation multicollector inductively coupled plasma mass spectrometry (LA-MC-ICPMS).

[11] The laser ICPMS analyses involve ablation of zircon with a New Wave DUV193 Excimer laser (operating at a wavelength of 193 nm) using a spot diameter of 25−35 microns. The ablated material is carried in argon gas into the plasma source of a Micromass Isoprobe, which is equipped with a flight tube of sufficient width that U, Th, and Pb isotopes are measured simultaneously. All measurements are made in static mode, using Faraday detectors for ^{238}U, ^{232}Th, $^{208-206}Pb$, and an ion-counting channel for ^{204}Pb. Ion yields are ∼1 mv per ppm. Each analysis consists of one 20-s integration on peaks with the laser off (for backgrounds), 20 1-s integrations with the laser firing, and a 30 s delay to purge the previous sample and prepare for the next analysis. The ablation pit is ∼20 microns in depth.

[12] Common Pb correction is performed by using the measured ^{204}Pb and assuming an initial Pb composition from *Stacey and Kramers* [1975] (with uncertainties of 1.0 for $^{206}Pb/^{204}Pb$ and 0.3 for $^{207}Pb/^{204}Pb$). Measurement of ^{204}Pb is unaffected by the presence of ^{204}Hg because backgrounds are measured on peaks (thereby subtracting any background ^{204}Hg and ^{204}Pb), and because very little Hg is present in the argon gas.

[13] For each analysis, the errors in determining $^{206}Pb/^{238}U$ and $^{206}Pb/^{204}Pb$ result in a measurement error of several percent (at 2σ level) in the $^{206}Pb/^{238}U$ age (Table 4). The errors in measurement of $^{206}Pb/^{207}Pb$ are substantially larger for younger grains due to low intensity of the ^{207}Pb signal. The $^{207}Pb/^{235}U$ and $^{206}Pb/^{207}Pb$ ages for younger grains accordingly have large uncertainties (Table 4). Interelement fractionation of Pb/U is generally <20%, whereas isotopic fractionation of Pb is generally <5%. Run analyses of fragments of a large zircon crystal (generally every fifth measurement) with known age of 564 ± 4 Ma (2σ error) are used to correct for this fractionation. The uncertainty resulting from the calibration correction is generally ∼3% (2σ) for both $^{207}Pb/^{206}Pb$ and $^{206}Pb/^{238}U$ ages.

[14] The ages interpreted from the ICPMS analyses are based on $^{206}Pb/^{238}U$ ratios because errors of the $^{207}Pb/^{235}U$ and $^{206}Pb/^{207}Pb$ ratios are significantly greater. This is due primarily to the low intensity (commonly <1 mV) of the ^{207}Pb signal from these young, U-poor grains. A comparison between ID-TIMS ages and laser ICPMS ages is available from sample 630-5, which was analyzed by both methods, and by a second zircon standard (00−87)

that was analyzed during the same session. The ID-TIMS age for 630-5 is 93 ± 3 Ma, whereas the laser ICPMS mean age is 92.0 ± 4.1 Ma (Figures 7 and 8). For sample 00–87, the ID-TIMS age is 99.2 ± 1.0 Ma, and the ICPMS $^{206}Pb/^{238}U$ age is 99.9 ± 3.3 Ma. We accordingly conclude that our reported $^{206}Pb/^{238}U$ ages are reliable indicators of crystallization age.

[15] Whole-rock sample 710-5 was broken down by hammer and crushed in a jaw crusher to about 1/3 of its average grain size. The sample was then homogenized and split, roughly two thirds for mineral separation, and a third for whole rock analysis. Both splits were initially washed in deionized water and then acid leached for 25–30 min in warm 1 N distilled HCl while in an ultrasonic bath. The whole-rock sample was then ground to a fine powder using a ceramic Al_2O_3 shatter box prior to dissolution. The split for mineral analyses remained relatively coarse throughout the separation procedure, although for some samples rich in composite grains, a few additional grinding steps were necessary. Separation of minerals was accomplished by a Frantz magnetic separator and handpicking in alcohol under a binocular microscope. Two garnet fractions were used, one corresponding optically to the slightly more orange colored mineral rims (gar-1), and the other one representing a mixture of the red and orange colors of the Cone Peak garnets. The samples were then ultrasonically cleaned, rinsed multiple times with ultrapure water and dried in methanol.

[16] The samples were spiked with mixed ^{147}Sm-^{150}Nd tracers described by *Ducea et al.* [2003c]. Dissolution of the spiked samples for isotopic analyses was performed in screw cap Teflon beakers using HF-HNO_3 (on hot plates) and HF-$HClO_4$ mixtures (in open beakers at room temperature). A few garnet separates were subjected to up to 5 dissolution steps before becoming residue free. The samples were taken in 1 N HCl and any undissolved residue was attacked using the HF-$HClO_4$ mixture digestion technique. Separation of the bulk of the REE was achieved via HCl elution in cation columns. Separation of Sm and Nd was carried out using a LNSpec® resin following the procedures in *Ducea et al.* [2003c].

[17] Mass spectrometric analyses were carried out on two VG Sector multicollector instruments (VG54 and VG354) fitted with adjustable 10^{11} Ω Faraday collectors and Daly photomultipliers [*Patchett and Ruiz*, 1987]. Concentrations of Sm and Nd were determined by isotope dilution. An off-line manipulation program was used for isotope dilution calculations. Typical runs consisted of 100 isotopic ratios. The mean results of five analyses of the standard nSmβ performed during the course of this study are: $^{148}Sm/^{147}Sm$ = 0.74880 ± 21, and $^{148}Sm/^{152}Sm$ = 0.42110 ± 6. Fifteen measurements of the LaJolla Nd standard were performed during the course of this study, yielding the following isotopic ratios: $^{142}Nd/^{144}Nd$ = 1.14184 ± 2, $^{143}Nd/^{144}Nd$ = 0.511853 ± 10, $^{145}Nd/^{144}Nd$ = 0.348390 ± 20, and $^{150}Nd/^{144}Nd$ = 0.23638 ± 2. The Nd isotopic ratios were normalized to $^{146}Nd/^{144}Nd$ = 0.7219. The estimated analytical ±2σ uncertainties for samples analyzed in this study are: $^{147}Sm/^{144}Nd$ = 0.4%, and $^{143}Nd/^{144}Nd$ = 0.001%. The isochron standard error and the Mean Squared Weighted Deviation (MSWD) were calculated using *Ludwig* [2001].

4. Geology of the Cone Peak Transect

[18] While the Sur Series rocks exposed in the study area have not previously been mapped in detail, they have been considered to be predominantly metasedimentary based on their banded appearance, the presence of marble and quartzite layers, and their proximity to the less metamorphosed rocks of the Salinian Central block. The rocks are predominantly in the amphibolite facies, with typical assemblages comprising plagioclase + hornblende + biotite ± quartz (in order of decreasing abundance). Granulite facies rocks and veins are also present, with typical assemblages comprising plagioclase + clinopyroxene ± biotite ± garnet ± quartz ± orthopyroxene. Small mappable gabbro and diorite intrusions were also found and comprise a significant portion of the study area. The igneous rocks typically share the above mineral assemblages with the gneisses and are distinguished based on remnant igneous textures and the near absence of marble and quartzite within the intrusions. Fine grained mafic rocks or "amphibolites" are also common in the gneiss and igneous rocks. We noted no differences between the fine-grained mafic rocks within the metamorphic framework and those within the igneous rocks. The metamorphic framework, igneous rocks, and fine-grained mafic rocks are discussed separately below. A detailed geologic map showing the study area and locations of the various rock types is shown in Figure 3.

4.1. Sur Series

[19] Metamorphic framework rocks in the study area vary greatly in composition and appearance. At outcrop scales, interlayered felsic gneisses, amphibolites, marbles and quartzites give the framework an overall banded appearance (Figure 4). Foliation measurements are variable (Figure 3b), showing significant scatter about an average WNW strike and 30° NE dip. Small outcrops and hand samples are often massive or show only a weak foliation due to low mica content, and mica-rich layers are negligible in the section. Veins are found in nearly all outcrops, and occasionally are concentrated enough to lend outcrops a migmatitic appearance. Felsic gneisses are the most common framework rocks and are composed primarily of plagioclase ± quartz ± biotite ± alkali feldspar ± garnet ± clinopyroxene ± hornblende ± orthopyroxene. Granoblastic fabrics are occasionally found, but high-temperature fabrics are more often overprinted by shear bands or weakly mylonitic fabrics. Quartz commonly shows undulatory extinction and significant recrystallization. The felsic gneisses have an average tonalitic composition but are split between two populations, one with an average diorite or quartz diorite composition, and the other with a tonalitic composition containing typically 50% quartz. The only unambiguous sedimentary units in the section are quartzites and marbles. Pure quartzites (>90% quartz) are quite rare in the gneiss, and are found

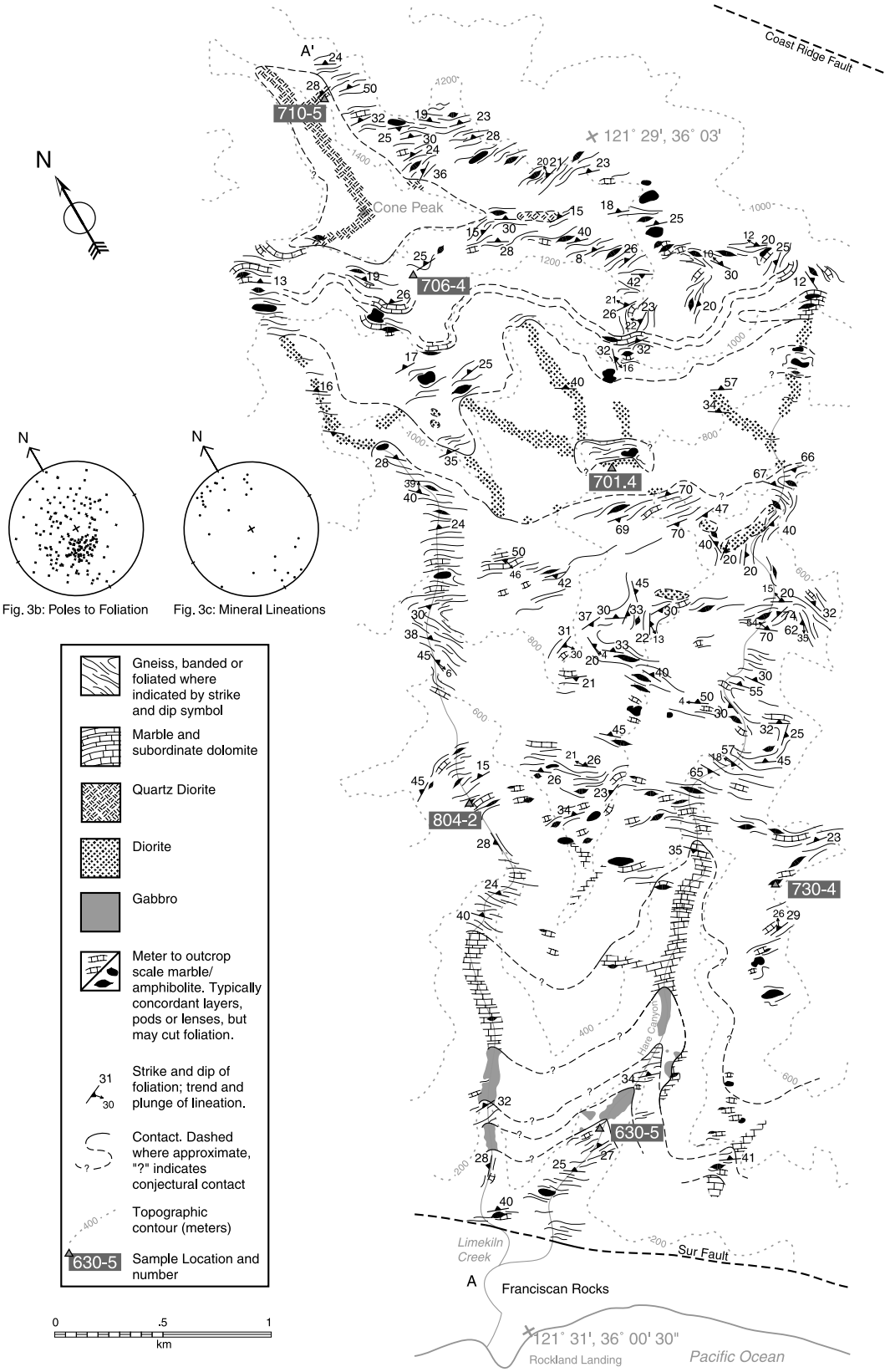
Coast Ridge Fault
A'
710-5
706-4
701.4
804-2
730-4
630-5
Cone Peak
121° 29', 36° 03'
N
Fig. 3b: Poles to Foliation
Fig. 3c: Mineral Lineations
Gneiss, banded or foliated where indicated by strike and dip symbol
Marble and subordinate dolomite
Quartz Diorite
Diorite
Gabbro
Meter to outcrop scale marble/ amphibolite. Typically concordant layers, pods or lenses, but may cut foliation.
Strike and dip of foliation; trend and plunge of lineation.
Contact. Dashed where approximate, "?" indicates conjectural contact
Topographic contour (meters)
Sample Location and number
0 .5 1
km
Limekiln Creek
A
Franciscan Rocks
Sur Fault
121° 31', 36° 00' 30"
Rockland Landing
Pacific Ocean

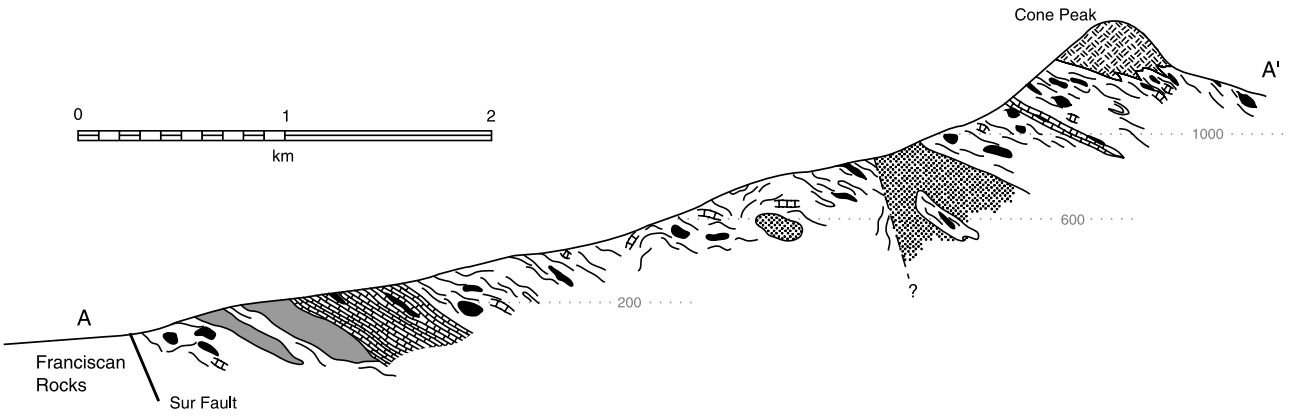

Figure 3. (continued)

only as cm-scale to dm-scale bodies. Pure quartzites were found only in the northern portion of the section. Less pure quartzites, occasionally graphite bearing, appear at meter scale here and there throughout the section but were not mapped due to their scarcity and small size. Some of the impure ''quartzites'' in the section may be igneous or hydrothermal in origin, as they are occasionally seen in crosscutting relations with other rocks.

[20] Marbles are widely scattered throughout the gneiss at a variety of scales, from layers a few cm in thickness to two map-scale layers (Figure 3). The marbles are generally concordant with foliation, although in one locality a meter-wide marble body is seen to cut foliation. This one marble probably formed during metamorphism from CO_2-rich fluids. The marble is generally a dirty gray color, fine grained and porphyroblastic. Occasionally it is found recrystallized to a pure, white, coarse-grained dolomite or marble where it is typically marked by the presence of olivine. Gneissic rocks and fine-grained mafic rocks are commonly associated with the marble as tubes, blobs, and isolated tight folds (e.g., Figure 5).

4.2. Plutonic Rocks

[21] Earlier mapping at larger scales [*Reich*, 1937; *Compton*, 1966b; *Seiders et al.*, 1983] did not distinguish four mafic to intermediate intrusions that occupy in cross-sectional thickness about a third of the study area. The intrusions comprise two hornblende gabbro sills in the southern portion of the mapped area, a diorite in the central portion, and a quartz diorite in the northern portion (Figure 3). Other mafic igneous rocks similar in texture and appearance to the larger bodies are found as dikes, veins, and outcrop-scale to small map-scale bodies in the gneiss. The contacts of the larger igneous bodies are generally gradational and concordant with folitation.

[22] Two concordant 100- to 200-m-thick gabbro sills found in the southern part of the mapped area comprise the most mafic igneous bodies found. The sills are quite heterogeneous, but generally comprise a mixture of two textural end members: a medium to coarse-grained variety with typically elongate subhedral hornblende crystals, and a fine-grained typically granoblastic variety. In places the fine-grained material appears as enclaves in the coarser-grained material, in other cases the coarser-grained material exists as patches and veins in the fine-grained material (Figure 6). Both varieties are also seen in cross cutting relationships with the other. While the fine-grained rocks maintain rather even ratios of felsic to mafic minerals, the coarser-grained rocks range from nearly 100% hornblende to a near total absence of hornblende in some veins. In thin section, coarse-grained samples generally contain subhedral or granoblastic hornblende crystals with feldspars showing granoblastic textures. Contacts between the gabbro and country rock were not observed due to thick cover, but mapping leaves generally less than 50 m for a diffuse transition zone (Figure 3).

[23] A roughly 500-m-thick diorite in the central part of the area comprises the largest igneous body mapped. The diorite is very heterogeneous, containing a multitude of fine-grained mafic enclaves and country rock inclusions. It is generally medium-grained with a granoblastic fabric, and typically contains 65–80% plagioclase + hornblende ± quartz. The intrusion thins significantly and is more felsic in the western portion of the mapped area. It is unclear

Figure 3. (opposite) (a) Geologic map of Hare Canyon and Cone Peak area showing location of units and samples discussed in the text. See Figure 2 for location. The gneiss unit is strewn with minor marble and fine-grained mafic layers, lenses, and blobs. The size of the symbols is intended as a rough indication of the size of the bodies; the larger symbols are shown to scale, however, smaller symbols represent bodies that may be as small as a few square m. The geometry of the bodies is commonly obscured by thick cover; thus the true shapes of the minor mafic and marble bodies may differ significantly from the shape of map symbols. Contacts separating the gneiss units from the quartz diorite and diorite bodies are often diffuse over as much as 300 m. (b) Stereoplot showing poles to all measured foliations. (c) Stereoplot showing mineral lineation directions. (d) Cross section from A to A′ in Figure 3a. Units are as shown in Figure 3a. There is no vertical exaggeration. Elevation is shown in m.

Figure 4. Coast Ridge Belt gneiss near Cone Peak. The upper part of the photograph shows the typical well-defined layering of the gneiss, cut by a rare mylonite comprising the lower third of the photograph. A thick quartzofeldspathic vein lies between the two foliations in the left-hand side of the photo. Asymmetric pressure shadows in the mylonite [*Passchier and Trouw*, 1998] and thinning in the gneiss suggest top to the right (east) offset. The thick, darker layer intersecting the top of the photograph is a typical small mafic body in the gneiss. The field of view is ~3.5 m.

Figure 5. Porphyroblastic marble showing z-shaped tightly folded quartzofeldspathic inclusion. The field of view is ~20 cm. The black material is lichen.

whether the thinning is a primary feature of the intrusive body or whether it is offset by a fault along the southern boundary of the intrusion.

[24] The unique, light-colored, generally banded to grossly isotropic biotite hornblende gneiss exposed at Cone Peak has been described in detail by *Compton* [1960] and by *Hansen and Stuk* [1993]. The body is interlayered at its base with quartzites and marbles, and neither *Compton* [1960] nor our own work revealed any cross cutting relationships involving the gneiss and country rocks. These and other observations led *Compton* [1960] to propose a sedimentary origin for the body. Zircons in the rock however are ~81 Ma (see below), signifying an igneous origin. This is supported by the quartz diorite composition of the Cone Peak gneiss, based on mineral modes and compositions estimated by us and *Hansen and Stuk* [1993].

4.3. Fine-Grained Mafic Rocks

[25] Fine-grained mafic rocks ranging in size from a few tens of cm to outcrop scale are widespread throughout all of the above igneous and metamorphic units. We found no systematic differences between samples derived from within the different rock types and thus we describe them here together. Most are amphibolites, with a groundmass containing the assemblage plagioclase + hornblende ± biotite. Veins in the amphibolite are widespread and often contain clinopyroxene in place of hornblende. Clinopyroxene replaces hornblende as the dominant mafic mineral in roughly a quarter of the fine-grained mafic rocks, thus many of them would be better termed pyroxenites. Biotite content varies in both types between 0 and 20%. Textures are generally granoblastic or partially granoblastic, with some grains showing serrated edges or other evidence of ductile deformation. Within the deformed framework these rocks most commonly comprise concordant layers or

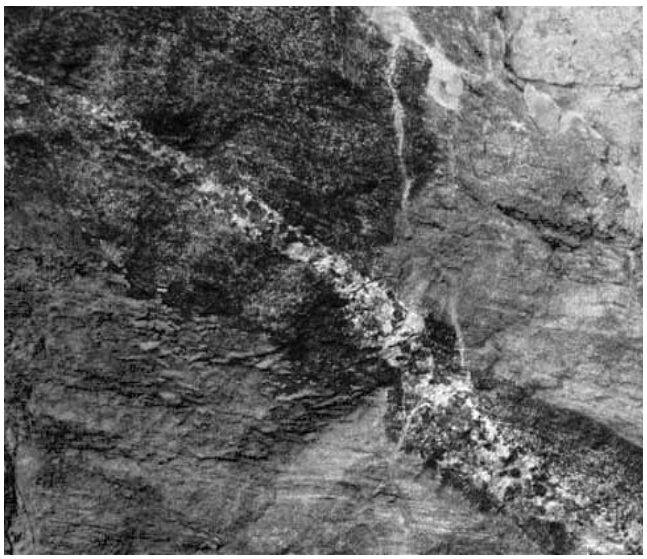

Figure 6. Photograph showing foliated quartzo-feldspathic layers (lower left and middle right side of photo) offset by fine-grained amphibolite material (darker material in areas between upper left and lower right corners of the photo). Such cross cutting relationships are quite unusual in the Coast Ridge Belt. The foliated amphibolite is overprinted by a more felsic, coarse-grained vein also running from upper left to lower right across the photograph. The field of view is about 1 m.

Table 2. Mineral Compositions for Geothermometry and Geobarometry

Sample Location	710-5 Core	710-5 Rim	730-4 Core	730-4 Rim	730-4 Included Core	730-4 Included Rim	804-2 Core	804-2 Rim	804-2 Included Core	804-2 Included Rim
					Garnets					
SiO_2	37.44	37.36	37.98	37.83	37.87	38.34	37.33	37.38	37.33	37.46
TiO_2	0.06	0.06	0.1	0.07	0.09	0.07	0.08	0.05	0.1	0.07
Al_2O_3	21.25	21.11	21.44	21.25	21.38	21.39	21.36	21.34	21.4	21.41
FeO	28.91	29.45	27.56	28.21	27.56	27.69	28.88	29.02	28.47	28.6
MnO	1.37	1.45	0.7	0.77	0.69	0.73	1.49	1.58	1.38	1.33
MgO	3.91	3.31	5.05	4.56	4.99	4.7	4.01	3.51	4.24	4.28
CaO	6.62	6.75	6.72	6.56	6.67	6.72	6.81	6.86	6.89	6.86
Na_2O	0	0.01	0.02	0.02	0.01	0.02	0.02	0.02	0.01	0.02
K_2O	0	0	0.01	0.01	0.01	0	0	0	0.01	0.01
Total	99.6	99.5	99.6	99.3	99.3	99.7	100	99.8	99.8	100
n[a]	3	4	10	3	5	8	13	16	12	10
					Clinopyroxenes					
SiO_2	50.13	50.98	51.94	51.79	52.48	51.45	51.77	51.78	51.01	51.3
TiO_2	0.23	0.2	0.23	0.2	0.13	0.03	0.08	0.13	0.24	0.19
Al_2O_3	1.73	1.43	2.18	1.74	1.64	1.51	0.87	1.04	1.71	1.48
FeO	15.46	15.11	13.03	12.26	12.39	12.54	12.76	13.29	13.47	12.96
MnO	0.33	0.31	0.14	0.14	0.13	0.12	0.23	0.28	0.27	0.25
MgO	9.51	10.23	12.66	11.73	12.14	11.94	11.57	11.56	11.15	11.58
CaO	20.86	20.92	18.18	20.72	20.78	20.72	22.02	21.3	21.1	21.42
Na_2O	0.35	0.33	0.3	0.32	0.4	0.37	0.24	0.27	0.37	0.34
K_2O	0	0.01	0.02	0.02	0	0.01	0.01	0.01	0	0.01
Total	98.6	99.5	98.7	98.9	100.1	98.7	99.6	99.7	99.3	99.5
n[a]	2	3	3	8	2	2	7	8	14	8
					Plagioclases[b]					
SiO_2	2.62	2.61	2.59	2.56	2.6	2.59	2.61	2.59	2.61	2.59
Al_2O_3	1.38	1.38	1.4	1.43	1.4	1.41	1.39	1.41	1.38	1.4
CaO	0.38	0.38	0.41	0.43	0.4	0.41	0.39	0.4	0.38	0.4
Na_2O	0.63	0.6	0.58	0.56	0.57	0.57	0.62	0.6	0.62	0.6
K_2O	0.01	0.02	0.03	0.02	0.03	0.02	0.01	0.01	0.02	0.03
Total	99	99.2	99.6	99.7	99.5	99.3	99.8	99.8	99.9	99.6
n[a]	2	3	6	11	4	2	10	5	8	5

[a]Number of analysis spots.
[b]Concentration of Ti, Fe, Mn, and Mg are <0.01.

lenses in the gneiss (e.g., Figure 4), although in places amphibolite dikes are seen to cut foliation (e.g., Figure 6).

4.4. Garnet Growth

[26] All of the Coast Ridge Belt rocks, with the exception of the carbonates, are commonly garnetiferous. The garnets are almandine rich, with X_{Al} ranging from 0.57 to 0.64 in rock types of a wide variety of compositions. They are commonly as large as 15 mm in diameter, although some exceptional specimens reach diameters as large as 10 cm. The garnets are typically poikiloblastic and overprint host rock fabrics, although in thin section foliation is often bent around garnets. Inclusions of feldspar, quartz, hornblende and pyroxene are common. Garnet is commonly associated in thin section and outcrop with aureoles or small, recrystallized veins in which clinopyroxene and quartz are common.

5. Thermobarometry

[27] Geothermometric and geobarometric estimates were made in two samples located near the southern portion of the area (730-4, 804-2) and in one sample located near Cone Peak (710-5). Temperature and pressure estimates were calculated using the rim and core compositions of touching garnet, clinopyroxene and plagioclase grains. Mineral compositions used are given in Table 2. Most of the garnets contain inclusions, and ''core'' garnet compositions were taken as far from inclusions as possible rather than strictly in the center of grains. Rim measurements were taken between 10 and 40 microns from interfaces with corresponding minerals. Temperatures were estimated using the *Ellis and Green* [1979] and *Ganguly et al.* [1996] calibrations of the garnet-clinopyroxene thermometer. Pressures were estimated using the *Eckert et al.* [1991] correction to *Newton and Perkins* [1982] garnet-clinopyroxene-plagioclase-quartz barometer. Core compositions yielded temperatures, with one exception, between 750 and 870°C at pressures of 0.75 GPa (see Table 3). Temperatures using the *Ganguly et al.* [1996] thermometer for each site are consistently 50°–70°C higher than those calculated using the *Ellis and Green* [1979] thermometer. Calculated pressures on mineral cores range from 0.66 GPa to 0.79 GPa at 750° or from 0.69 to 0.82 GPa at 800°C. Analyzed garnet and clinopyroxene crystals show a slight zoning in the outer 50–100 microns, and conditions based

Table 3. Results of Geothermometry and Geobarometry[a]

Sample	T_E	T_G	P_E^{750}	P_E^{800}
710-5 core	863	806	0.73	0.76
710-5 rim	790	728	0.65	0.67
730-4 core	822	761	0.79	0.82
730-4 rim	793	727	0.74	0.77
730-4 inclusion core	817	755	0.75	0.78
730-4 inclusion rim	808	747	0.73	0.76
804-2 core	771	705	0.66	0.69
804-2 rim	749	684	0.62	0.65
804-2 inclusion core	811	750	0.73	0.76
804-2 inclusion rim	793	730	0.69	0.72

[a]Temperatures are measured in °C; pressures are measured in GPa. Superscript indicates temperatures (750°C or 800°C) at which pressures were calculated. Temperatures were calculated at 0.75 GPa. T_G, *Ganguly et al.* [1996]; T_E, *Ellis and Green* [1979]; P_E = *Eckert et al.* [1991].

on rim compositions are on average 30°–40°C and 0.05 GPa below peak conditions. The rim and core results are indistinguishable given the uncertainties of the calibrations. We take ranges of 750°–800°C and 0.7–0.8 GPa as the best estimates of peak metamorphic conditions recorded in the study area. These results are similar to results reported by *Hansen and Stuk* [1993] from Cone Peak as well as to conditions obtained on rocks from the two other California deeper arc exposures, the Tehachapi section [*Pickett and Saleeby*, 1993] and the Cucamonga section [*Barth and May*, 1992]. Undoubtedly, the intrusion temperatures were higher than these measured values, given the intermediate and/or mafic composition of the investigated rocks. The results correspond to an average thermal gradient of ~30°C/km which is typical for active continental arcs [*Barton*, 1990].

6. Geochronology

6.1. U/Pb Zircon Results

[28] Zircons from the Coast Ridge Belt samples were analyzed optically under a petrographic microscope and an SEM in BSE mode. Zircons were grouped according to the morphology classification of *Pupin* [1983]. Almost all zircons that yielded Cretaceous ages display igneous morphologies with no detectable optical zoning. The older zircons we found particularly in sample 706-4, are smaller, rounded grains that indicate a detrital origin and/or corrosion in a magma. For these zircons, we report the core ages that are always older than rim ages. Rim ages are typically poorly constrained (probably because the new rim growths are very narrow), and are not reported in Table 4, but the ages are late Cretaceous.

6.1.1. Sample 630-5, Felsic Framework

[29] Eight single zircon grains were analyzed by ID-TIMS, three of which are discordant and five of which are apparently concordant (Figure 7). The interpreted age derived from the concordant grains is 93 ± 3 Ma (2σ level). Thirty-nine grains were analyzed by ICPMS, with 33 analyses that yield a weighted mean age of 92.0 ± 4.1 Ma (2σ error) and a standard error of the mean of 1.7 Ma (Figure 8). The additional grains yield $^{206}Pb/^{238}U$ ages that range from ~110 to ~283 Ma, presumably due to the presence of inherited components.

6.1.2. Sample 701-4, Diorite

[30] Thirty grains were analyzed from this sample, with 23 grains that do not show sign of inheritance (Table 4). The weighted mean age is 86.4 ± 4.7 Ma (2σ error), with a standard error of the mean of 3.3 Ma (Figure 9). The additional seven grains are slightly older, presumably due to the presence of inherited components.

6.1.3. Sample 706-4, Quartz Diorite Gneiss

[31] Fifty-one grains were analyzed from this sample. Twenty-two grains yield a cluster of <90 Ma ages, with a weighted mean age of 81.3 ± 3.4 Ma (2σ error) and a standard error of the mean of 1.0 Ma (Table 4 and Figure 10). Twenty-nine grains yield mainly Paleozoic and Proterozoic ages due to inheritance of older components (Figure 11). As shown in Figure 11, the main $^{207}Pb/^{206}Pb$ age clusters of these inherited components are ~120 Ma, ~360 Ma, 1.0–1.25 Ga, ~1.4 Ga, ~1.6 Ga. The sample was taken from an area below the main body of the gneiss where the quartz diorite is intermingled with the Sur Series.

6.2. Sm-Nd Garnet Geochronology

[32] A six point Sm-Nd mineral and whole-rock isochron (Figure 12) obtained on a typical sample of the Cone Peak quartz diorite gneiss (sample 710-5) yielded an age of 76.5 ± 1.5 Ma, within the errors of the igneous crystallization age. Minerals and whole-rock Sm and Nd isotope data are shown in Table 5. Two garnet fractions (rims "gar-1" and whole garnets) were analyzed; and both lie on the same isochron, suggesting a fast growth rate (>4 mm/My). The closure temperature for the Sm-Nd system in garnet from this rock is about 760°C using diffusion data from *Ganguly and Tirone* [1999], similar but slightly less than the temperature recorded in the same sample by major cation exchange (800°–860°C). There are two possible explanations for the relationships between temperatures and the age recorded in this rock: (1) the age records garnet growth, in which case the Cone Peak rocks are shown to have been at depths of ~25 km at 76.5 Ma, or (2) the age records cooling through the ~760°C isotherm, in which case the age is a minimum for garnet growth. Given the fast cooling of this rock evidenced by the lack of significant zoning in garnets, and the overlapping error bars of the two temperature estimates, we favor the first interpretation. Although foliation in thin section can be seen to bend slightly around garnets in this rock, the garnets overprint the gross foliation of the sample, suggesting that garnet growth was late kinematic to postkinematic. This date therefore brackets in either of the above cases the timing of foliation-forming deformation of the Cone Peak quartz diorite to between crystallization at 81.3 ± 3.4 Ma and 76.5 ± 1.5 Ma. These dates also bracket peak metamorphic conditions measured on the Cone Peak rocks [*Hansen and Stuk*, 1993] (this study).

6.3. Other Age Constraints

[33] The Cone Peak rocks were exposed at the surface by mid-Maastrichtian (~68–69 Ma), as indicated by the age of sedimentary rocks unconformably overlying the Coast Ridge

Table 4. U-Pb Geochronologic Analyses by Laser-Ablation Multicollector ICP Mass Spectrometery[a]

				Isotopic Ratios			Apparent Ages, Ma		
Sample	U, ppm	$^{206}Pb/^{204}Pb$	U/Th	$^{207}Pb/^{235}U$ (±, %)	$^{206}Pb/^{238}U$ (±, %)	Error Correlation	$^{206}Pb/^{238}U$ (±, Ma)	$^{207}Pb/^{235}U$ (±, Ma)	$^{206}Pb/^{207}Pb$ (±, Ma)
				Sample 630-5					
1	4	325	0.4	0.10044 (272.6)	0.01360 (9.2)	0.03	87.1 (8.1)	97 (246)	353 (3078)
2	4	334	2	0.29122 (40.4)	0.01455 (4.3)	0.11	93.1 (4.0)	260 (113)	2290 (346)
3	6	243	5	0.03161 (70.8)	0.01396 (11.3)	0.16	89.3 (10.1)	32 (23)	
4	5	112	11	0.04878 (131.4)	0.01103 (21.1)	0.16	70.7 (15.0)	48 (63)	
5	5	229	11	0.02313 (97.7)	0.01229 (22.2)	0.23	78.7 (17.6)	23 (23)	
6	5	210	2	0.28004 (110.1)	0.01428 (3.5)	0.03	91.4 (3.2)	251 (273)	2254 (950)
7	*12*	*1120*	*8*	*0.36837* (*13.0*)	*0.04076* (*3.7*)	*0.29*	*257.5* (*9.8*)	*318* (*47*)	*792* (*130*)
8	4	426	8	0.10031 (72.2)	0.01432 (7.8)	0.11	91.7 (7.2)	97 (71)	232 (828)
9	5	300	2	0.04636 (100.4)	0.01431 (10.9)	0.11	91.6 (10.0)	46 (46)	
10	*63*	*6572*	*99*	*0.62605* (*2.8*)	*0.04493* (*1.2*)	*0.44*	*283.3* (*3.6*)	*494* (*18*)	*1644* (*23*)
11	*7*	*499*	*2*	*1.24496* (*0.0*)	*0.01766* (*5.4*)	*0.02*	*112.9* (*6.1*)	*821* (*1359*)	*4274* (*1662*)
12	*15*	*1014*	*7*	*0.05806* (*45.1*)	*0.01954* (*3.4*)	*0.08*	*124.7* (*4.3*)	*57* (*26*)	
13	6	378	4	0.02821 (92.9)	0.01530 (8.1)	0.09	97.9 (8.0)	28 (26)	
14	4	275	5	0.05365 (149.8)	0.01331 (14.4)	0.10	85.2 (12.3)	53 (79)	
15	4	222	5	0.28819 (85.2)	0.01346 (10.2)	0.12	86.2 (8.8)	257 (223)	2405 (719)
16	3	510	12	0.04599 (339.6)	0.01543 (12.9)	0.04	98.7 (12.8)	46 (147)	
17	4	580	27	0.06282 (121.5)	0.01475 (2.5)	0.02	94.4 (2.3)	62 (75)	
18	18	693	8	0.34999 (116.4)	0.01404 (4.5)	0.04	89.9 (4.1)	305 (347)	2660 (964)
19	17	213	37	0.05883 (24.9)	0.01363 (3.1)	0.13	87.2 (2.8)	58 (15)	
20	10	263	9	0.22115 (103.3)	0.01452 (5.0)	0.05	92.9 (4.7)	203 (209)	1807 (938)
21	25	635	9	0.14426 (35.7)	0.01504 (2.0)	0.06	96.2 (2.0)	137 (51)	916 (366)
22	9	265	8	−0.02096 (266.6)	0.01364 (7.1)	0.03	87.3 (6.3)	−22 (−58)	
23	*17*	*810*	*11*	*0.08917* (*21.8*)	*0.01754* (*3.1*)	*0.14*	*112.1* (*3.5*)	*87* (*20*)	
24	14	574	5	0.44737 (189.6)	0.01445 (2.5)	0.01	92.5 (2.3)	375 (624)	3014 (1522)
25	18	506	22	0.13621 (50.2)	0.01546 (4.6)	0.09	98.9 (4.6)	130 (67)	738 (529)
26	7	153	4	0.95721 (433.4)	0.01556 (7.7)	0.02	99.5 (7.8)	682 (1664)	4073 (3225)
27	*13*	*1221*	*7*	*0.09090* (*51.9*)	*0.01883* (*3.0*)	*0.06*	*120.3* (*3.6*)	*88* (*47*)	
28	16	547	7	0.09058 (97.3)	0.01393 (3.7)	0.04	89.2 (3.3)	88 (86)	58 (1160)
29	8	173	24	0.02126 (95.5)	0.01266 (6.7)	0.07	81.1 (5.5)	21 (20)	
30	10	841	7	0.06497 (32.6)	0.01627 (5.5)	0.17	104.0 (5.8)	64 (21)	
31	12	131	13	0.08849 (141.3)	0.01271 (4.1)	0.03	81.4 (3.4)	86 (120)	217 (1635)
32	7	219	6	−0.00611 (116.1)	0.01372 (7.2)	0.06	87.9 (6.3)	−6 (−7)	
33	14	592	9	0.09075 (10.0)	0.01406 (4.5)	0.45	90.0 (4.1)	88 (9)	40 (107)
34	10	431	6	0.23671 (82.9)	0.01346 (5.9)	0.07	86.2 (5.1)	216 (182)	2064 (729)
35	16	524	8	0.17552 (82.1)	0.01480 (2.3)	0.03	94.7 (2.2)	164 (137)	1339 (793)
36	9	414	16	0.05388 (76.4)	0.01478 (5.4)	0.07	94.6 (5.2)	53 (41)	
37	7	155	2	0.13514 (44.7)	0.01335 (8.4)	0.19	85.5 (7.2)	129 (60)	1025 (444)
38	10	329	4	0.31884 (88.6)	0.01507 (6.1)	0.07	96.4 (5.9)	281 (253)	2385 (752)
39	8	642	5	0.37378 (109.9)	0.01221 (27.0)	0.25	78.2 (21.2)	323 (350)	2995 (857)
				Sample 701-4					
1	3	235	15	0.05656 (102.0)	0.01347 (10.2)	0.10	86.3 (8.8)	56 (57)	
2	*4*	*452*	*2*	*0.15748* (*207.5*)	*0.01915* (*19.3*)	*0.09*	*122.3* (*23.7*)	*149* (*287*)	*591* (*2240*)
3	5	496	1	0.03840 (50.3)	0.01385 (9.8)	0.20	88.7 (8.8)	38 (19)	
4	4	522	3	0.20372 (34.9)	0.01338 (8.4)	0.24	85.7 (7.2)	188 (70)	1806 (308)
5	*1*	*553*	*68*	*0.21125* (*169.8*)	*0.01845* (*27.7*)	*0.16*	*117.9* (*32.8*)	*195* (*311*)	*1270* (*1635*)
6	5	240	52	0.10077 (53.3)	0.01310 (7.8)	0.15	83.9 (6.6)	98 (53)	444 (586)
7	6	344	4	0.06718 (190.4)	0.01298 (9.9)	0.05	83.2 (8.3)	66 (122)	−519 (2541)
8	*5*	*251*	*7*	*0.14558* (*55.2*)	*0.01693* (*11.2*)	*0.20*	*108.2* (*12.2*)	*138* (*78*)	*687* (*576*)
9	7	289	10	0.04085 (50.2)	0.01427 (8.5)	0.17	91.4 (7.8)	41 (21)	
10	*5*	*240*	*5*	*0.22678* (*105.8*)	*0.01935* (*7.5*)	*0.07*	*123.6* (*9.3*)	*208* (*218*)	*1315* (*1024*)
11	4	321	2	0.20869 (47.3)	0.01403 (7.7)	0.16	89.8 (6.9)	193 (96)	1764 (426)
12	8	322	19	0.19355 (60.6)	0.01338 (6.1)	0.10	85.7 (5.2)	180 (113)	1713 (555)
13	4	396	6	0.06872 (111.3)	0.01353 (12.9)	0.12	86.7 (11.3)	68 (75)	
14	4	130	7	0.06841 (98.8)	0.01153 (22.0)	0.22	73.9 (16.4)	67 (66)	−165 (1199)
15	6	270	3	0.29754 (73.3)	0.01374 (8.5)	0.12	87.9 (7.5)	265 (200)	2425 (617)
16	*5*	*299*	*11*	*0.14960* (*30.4*)	*0.03108* (*9.0*)	*0.30*	*197.3* (*18.0*)	*142* (*45*)	
17	*2*	*702*	*26*	*0.07860* (*42.4*)	*0.02280* (*11.3*)	*0.27*	*145.3* (*16.6*)	*77* (*33*)	
18	5	356	1	0.16716 (59.3)	0.01342 (8.8)	0.15	86.0 (7.6)	157 (96)	1432 (559)
19	5	196	9	0.30266 (70.3)	0.01460 (7.3)	0.10	93.4 (6.9)	269 (196)	2350 (598)
20	4	150	17	0.00005 (41.7)	0.01223 (9.7)	0.23	78.4 (7.6)		
21	2	195	22	0.04127 (55.3)	0.01396 (8.3)	0.15	89.4 (7.5)	41 (23)	
22	*5*	*185*	*5*	*0.33444* (*87.6*)	*0.01775* (*6.3*)	*0.07*	*113.4* (*7.2*)	*293* (*261*)	*2186* (*760*)
23	7	306	7	0.11393 (42.4)	0.01286 (11.0)	0.26	82.4 (9.1)	110 (48)	750 (433)
24	8	325	14	0.08520 (97.9)	0.01380 (7.3)	0.07	88.4 (6.5)	83 (81)	

Table 4. (continued)

Sample	U, ppm	$^{206}Pb/^{204}Pb$	U/Th	Isotopic Ratios			Apparent Ages, Ma		
				$^{207}Pb/^{235}U$ (±, %)	$^{206}Pb/^{238}U$ (±, %)	Error Correlation	$^{206}Pb/^{238}U$ (±, Ma)	$^{207}Pb/^{235}U$ (±, Ma)	$^{206}Pb/^{207}Pb$ (±, Ma)
25	8	307	8	0.56804 (120.5)	0.01299 (10.6)	0.09	83.2 (8.9)	457 (529)	3556 (924)
26	8	222	18	0.15959 (77.8)	0.01335 (7.3)	0.09	85.5 (6.3)	150 (119)	1354 (747)
27	3	201	18	0.07505 (98.5)	0.01281 (16.1)	0.16	82.1 (13.3)	74 (72)	
28	2	385	20	0.06942 (104.4)	0.01136 (53.1)	0.51	72.8 (38.8)	68 (71)	
29	4	702	88	0.13393 (45.2)	0.01396 (9.0)	0.20	89.4 (8.1)	128 (60)	916 (456)
30	2	268	22	0.06219 (80.3)	0.01248 (30.5)	0.38	79.9 (24.5)	61 (50)	
				Sample 706-4					
1	*35*	*5514*	*18*	*1.37402 (3.0)*	*0.12674 (1.0)*	*0.34*	*769.2 (8.3)*	*878 (41)*	*1163 (28)*
2	*7*	*2085*	*5*	*1.53218 (7.9)*	*0.15177 (1.3)*	*0.16*	*910.9 (12.2)*	*943 (116)*	*1020 (79)*
3	75	1909	30	0.07635 (10.4)	0.01242 (1.0)	0.10	79.6 (0.8)	75 (8)	
4	*20*	*6437*	*8*	*1.13721 (2.7)*	*0.11220 (1.2)*	*0.45*	*685.5 (8.8)*	*771 (31)*	*1028 (24)*
5	*23*	*16757*	*8*	*3.25940 (1.5)*	*0.23337 (0.8)*	*0.55*	*1352.1 (12.1)*	*1471 (48)*	*1648 (11)*
6	*124*	*4817*	*842*	*0.46022 (8.5)*	*0.05676 (2.4)*	*0.28*	*355.9 (8.8)*	*384 (39)*	*560 (89)*
7	*22*	*6612*	*9*	*2.11498 (3.6)*	*0.16850 (1.7)*	*0.47*	*1003.8 (18.0)*	*1154 (74)*	*1447 (30)*
8	*22*	*4173*	*21*	*1.34860 (3.4)*	*0.10493 (2.8)*	*0.83*	*643.2 (18.9)*	*867 (45)*	*1492 (18)*
9	*67*	*1809*	*934*	*0.14407 (12.9)*	*0.01872 (1.6)*	*0.12*	*119.6 (1.9)*	*137 (19)*	*445 (142)*
10	*25*	*6549*	*9*	*2.00399 (1.9)*	*0.18427 (1.2)*	*0.64*	*1090.3 (14.0)*	*1117 (37)*	*1169 (14)*
11	*8*	*3180*	*9*	*2.14251 (7.6)*	*0.16566 (1.0)*	*0.13*	*988.1 (10.6)*	*1163 (154)*	*1504 (71)*
12	*5*	*1799*	*13*	*1.08937 (18.6)*	*0.10388 (4.2)*	*0.23*	*637.1 (28.3)*	*748 (188)*	*1097 (181)*
13	90	3360	1961	0.07782 (14.8)	0.01252 (0.8)	0.06	80.2 (0.7)	76 (12)	
14	16	615	13	0.09104 (47.7)	0.01203 (3.6)	0.08	77.1 (2.8)	89 (43)	408 (531)
15	111	13696	166	0.08977 (10.0)	0.01297 (0.9)	0.09	83.0 (0.8)	87 (9)	205 (115)
16	30	1280	9	0.08007 (27.5)	0.01220 (2.7)	0.10	78.2 (2.1)	78 (22)	79 (325)
17	*29*	*6249*	*21*	*0.13313 (65.5)*	*0.01803 (1.8)*	*0.03*	*115.2 (2.1)*	*127 (85)*	*352 (740)*
18	31	1797	10	0.10388 (71.9)	0.01360 (1.6)	0.02	87.0 (1.4)	100 (73)	429 (801)
19	32	1066	12	0.08349 (49.5)	0.01288 (2.2)	0.04	82.5 (1.8)	81 (41)	50 (590)
20	*9*	*5602*	*5*	*1.89499 (3.7)*	0.16902 (3.4)	*0.91*	*1006.7 (36.5)*	*1079 (69)*	*1229 (15)*
21	*99*	*3415*	*654*	*0.16051 (6.2)*	*0.01908 (1.1)*	*0.17*	*121.8 (1.3)*	*151 (10)*	*640 (66)*
22	*7*	*37107*	*4*	*1.79297 (8.3)*	*0.14673 (1.6)*	*0.19*	*882.6 (14.6)*	*1043 (141)*	*1396 (78)*
23	*20*	*6043*	*12*	*1.41734 (3.3)*	*0.12759 (1.1)*	*0.35*	*774.1 (9.2)*	*896 (46)*	*1211 (30)*
24	*26*	*9068*	*13*	*1.49968 (2.7)*	*0.13538 (1.6)*	*0.59*	*818.5 (13.9)*	*930 (41)*	*1205 (22)*
25	*54*	*5514*	*192*	*0.47149 (8.2)*	*0.05999 (0.7)*	*0.08*	*375.6 (2.6)*	*392 (39)*	*492 (90)*
26	*44*	*16285*	*13*	*1.14974 (2.8)*	*0.09500 (1.2)*	*0.42*	*585.0 (7.1)*	*777 (32)*	*1378 (24)*
27	24	2690	17	0.22569 (111.1)	0.01279 (2.9)	0.03	81.9 (2.4)	207 (227)	2071 (979)
28	25	1573	15	0.11656 (45.9)	0.01329 (3.6)	0.08	85.1 (3.0)	112 (53)	729 (485)
29	26	4300	16	0.08734 (31.4)	0.01265 (2.4)	0.08	81.1 (1.9)	85 (28)	198 (364)
30	19	2872	14	0.18753 (87.0)	0.01375 (4.7)	0.05	88.0 (4.1)	175 (153)	1604 (810)
31	16	1099	16	0.10290 (82.6)	0.01269 (4.5)	0.05	81.3 (3.7)	99 (83)	559 (899)
32	16	753	3	0.07485 (165.2)	0.01271 (4.2)	0.03	81.4 (3.4)	73 (118)	
33	*52*	*13620*	*22*	*0.14732 (27.3)*	*0.01507 (1.5)*	*0.06*	*96.4 (1.5)*	*140 (40)*	*955 (279)*
34	18	1585	0	0.09171 (46.1)	0.01284 (3.6)	0.08	82.3 (3.0)	89 (42)	276 (526)
35	*39*	*2379*	*8*	*0.12041 (27.7)*	*0.01497 (1.5)*	*0.05*	*95.8 (1.4)*	*115 (33)*	*542 (302)*
36	*14*	*4986*	*13*	*0.18489 (80.3)*	*0.01909 (2.8)*	*0.03*	*121.9 (3.4)*	*172 (141)*	*935 (823)*
37	*54*	*7565*	*298*	*0.16028 (13.4)*	*0.01566 (1.3)*	*0.10*	*100.2 (1.3)*	*151 (22)*	*1048 (134)*
38	49	5517	210	0.11080 (34.1)	0.01313 (1.6)	0.05	84.1 (1.3)	107 (38)	647 (366)
39	*22*	*1587*	*119*	*0.16187 (141.3)*	*0.01778 (2.5)*	*0.02*	*113.6 (2.8)*	*152 (209)*	*807 (1479)*
40	*49*	*7230*	*159*	*0.28380 (6.2)*	*0.03020 (1.6)*	*0.27*	*191.8 (3.2)*	*254 (18)*	*873 (61)*
41	*63*	*18885*	*576*	*0.20397 (8.0)*	*0.02029 (1.5)*	*0.19*	*129.5 (1.9)*	*189 (16)*	*1011 (79)*
42	*35*	*2813*	*3*	*0.13659 (108.3)*	*0.01458 (1.1)*	*0.01*	*93.3 (1.1)*	*130 (140)*	*867 (1123)*
43	24	23582	4	0.12177 (26.8)	0.01353 (3.3)	0.12	86.6 (2.9)	117 (33)	783 (279)
44	44	2296	108	0.09242 (29.0)	0.01254 (1.8)	0.06	80.3 (1.5)	90 (27)	349 (327)
45	68	2495	227	0.08972 (19.8)	0.01255 (1.6)	0.08	80.4 (1.3)	87 (18)	278 (226)
46	82	6676	353	0.09038 (12.6)	0.01274 (1.0)	0.08	81.6 (0.8)	88 (12)	261 (144)
47	94	3327	320	0.08428 (15.2)	0.01299 (2.9)	0.19	83.2 (2.4)	82 (13)	52 (178)
48	70	4958	133	0.08628 (10.3)	0.01250 (1.1)	0.11	80.1 (0.9)	84 (9)	198 (119)
49	*87*	*17697*	*776*	*0.19282 (7.3)*	*0.01575 (1.3)*	*0.17*	*100.7 (1.3)*	*179 (14)*	*1400 (69)*
50	*67*	*16909*	*3861*	*0.23801 (6.3)*	*0.01705 (2.1)*	*0.33*	*109.0 (2.3)*	*217 (15)*	*1647 (55)*
51	76	10608	1097	0.08861 (17.9)	0.01182 (2.9)	0.17	75.8 (2.2)	86 (16)	386 (198)

[a]Analyses in italics are not used in age calculations. All errors are at 1σ level and include only uncertainties in the measurement of isotope ratios. Systematic errors would add an additional ~2% (1σ) to each age. U concentration and U/Th have uncertainty of ~25%. Decay constants: $^{235}U = 9.8485 \times 10^{-10}$; $^{238}U = 1.55125 \times 10^{-10}$; $^{238}U/^{235}U = 137.88$. Isotope ratios are corrected for Pb/U fractionation by comparison with standard zircon with an age of 564 ± 4 Ma (2σ). Common Pb correction from measured $^{206}Pb/^{204}Pb$, with initial Pb composition interpreted from *Stacey and Kramers* [1975]. Uncertainties assigned to common Pb are 1.0 for $^{206}Pb/^{204}Pb$ and 0.3 for $^{207}Pb/^{204}Pb$ (2σ). $^{206}Pb/^{204}Pb$ is measured ratio. All other ratios are corrected for common Pb.

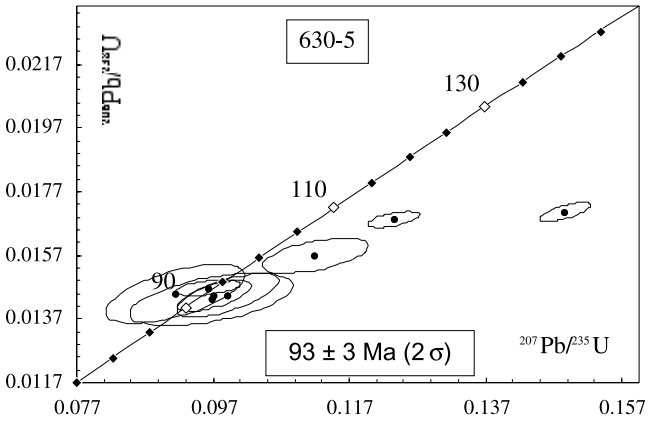

Figure 7. Conventional Concordia diagram showing ID-TIMS U/Pb results for sample 630-5.

Belt [*Saul*, 1986; *Seiders*, 1986; *Sliter*, 1986]. As described above, garnet growth at pressures of .75 GPa is bracketed between 81 ± 3 and 76 ± 1 Ma, and these results document 25 km of exhumation from between 81 and 76 and 68 Ma, corresponding to a rate of at least 1.9–3.1 km/my. *Naeser and Ross* [1976] reported a 71 Ma apatite fission track age (closure temperature of ~110°C) from rocks near Cone Peak. *Compton* [1966b] reported a K-Ar age of 75 ± 4 Ma from biotite in a sample collected at Cone Peak (closure temperature ~300°C). U-Th/He ages on rocks from the area mapped in this study [*Ducea et al.*, 2003a] are late Cenozoic (2–8 Ma), and when considered with the fission track data, indicate that the Coast Ridge Belt was buried by ~2–3 km of Cenozoic sediments. *Ducea et al.* [2003a] attribute exhumation in the late Cenozoic to transpressional tectonics related to the northward transport of Salinia.

7. Structures

[34] The rocks of the Coast Ridge Belt show evidence of deformation at a wide range of temperatures. Low-temperature brittle deformation everywhere overprints earlier mid-temperature or high-temperature deformation, and most rocks in the section show some evidence of brittle deformation. In thin section zones of crushed grains and deformation twins in calcite and feldspars are common. Hundreds of slickensides and slickenlines were also observed in outcrops throughout the study area. *Compton* [1966a] provided a detailed analysis of the brittle deformation features in the Santa Lucia range, and linked them to a long history of deformational events throughout the Pliocene and Pleistocene.

[35] The most common medium temperature features are mineral lineations present in nearly all quartzites or quartz-rich rocks, and mylonitic textures found occasionally in felsic rocks. The generally layer-parallel lineations are born primarily by elongate quartz grains and show a NNW-SSE preferred orientation (Figure 3c). In thin section, the elongate quartz grains typically show undulose extinction and are

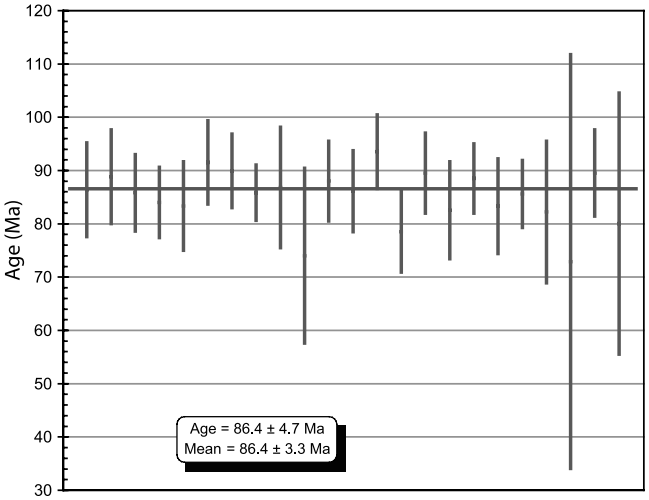

Figure 9. ICPMS ages and errors for single zircon crystals from sample 701-4.

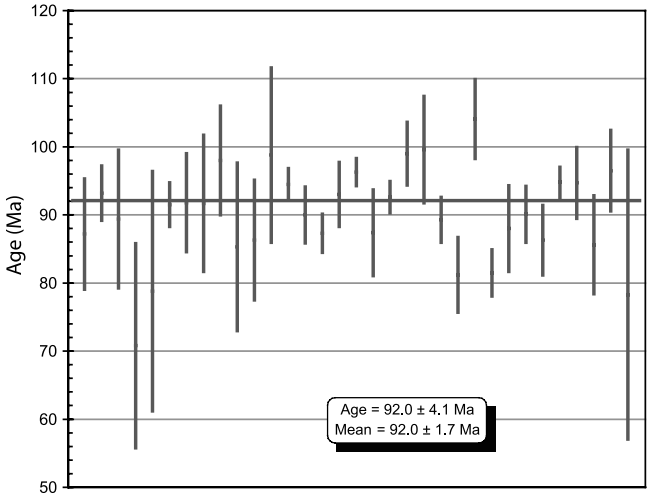

Figure 8. ICPMS ages and errors for single zircon crystals from sample 630-5.

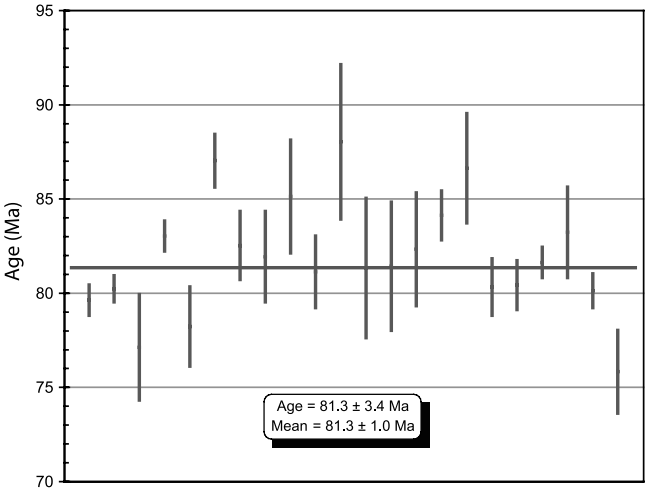

Figure 10. ICPMS ages and errors for single zircon crystals from sample 706-4.

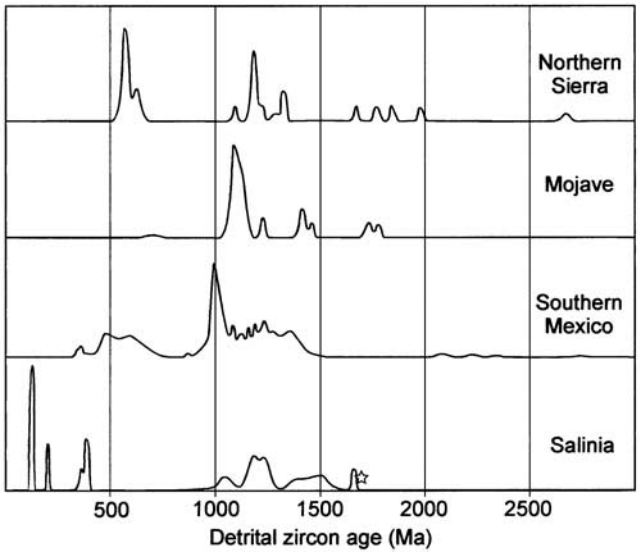

Figure 11. Relative age-probability curve of inherited zircon ages in sample 706-4 (“Salinia”). The star indicates the age of a Concordia diagram upper intercept (1.7 Ma) on “Sur Series” rocks at Ben Lomond Mountain, interpreted by *James and Mattinson* [1988] to represent inheritance age. The curve for <100 Ma Salinia grains has been removed so that the other curves are visible. Similar curves for the Sierra City mélange (“Northern Sierra” [*Harding et al.*, 2000]), the Wood Canyon formation of southern California (“Mojave” [*Stewart et al.*, 2001]), and lower Paleozoic strata from Acatlan and Oaxaca (“southern Mexico” [*Gillis et al.*, 2001; G. Gehrels, unpublished data, 2002] are shown for comparison.

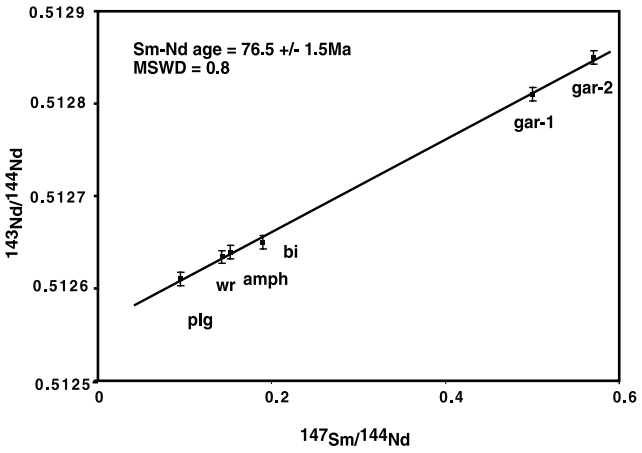

Figure 12. Six-point Sm-Nd mineral and whole-rock isochron, sample 710-5.

rimmed or nearly completely overgrown by small, recrystallized grains. The quartzite textures are comparable to dislocation creep regimes 2 and 3 of *Hirth and Tullis* [1992], which are typical of rocks deformed at midgreenschist and higher metamorphic grades [*Hirth and Tullis*, 1992]. Quartz also shows undulose extinction and strong recrystallization when present in less quartz-rich rocks. Most commonly the quartz fabrics are associated only with minor deformation of other minerals (e.g., deformation twins in feldspars). In a few samples however a weakly mylonitic texture is evident. Strong mylonitic fabrics are rare in the section but a few small patches of mylonitic rocks were found, in one case associated with ductile thinning of the layered gneiss outcrop shown in Figure 4. No map-scale relationships were evident linking areas of mylonitized rocks. Deformation at medium temperatures may also have been responsible for gentle outcrop-scale folds observed in the study area, although these folds may also have been formed at high temperatures. These ductile folds are partially responsible for the variation in foliation observed in the mapped area and depicted in Figure 3b.

[36] We propose that the overall banded nature of the Coast Ridge Belt is a structural feature resulting from the high-strain transposition of originally larger and more continuous preexisting units. The evidence for a high-strain structural origin of the banding is as follows: (1) Isoclinal folds are found in the section, (2) At both map and outcrop scale, foliation is generally defined by lenses or pods of diverse lithologies rather than semicontinuous layers. For example, two large marble bodies in the Coast Ridge Belt have thicknesses of ~1 km, but extend only 2–3 km in the plane of foliation [see *Ross*, 1976]. (3) Intrusive, metaigneous material is common throughout the gneiss (see discussion below), however there is a near-complete absence of cross cutting relationships. A high-strain environment is required to create such features. Three observations suggest that this fabric developed at high temperatures: (1) medium-temperature deformation features such as mylonitic fabrics are scarce, (2) many deformed mafic lenses or layers, show near equilibrium textures in thin section, suggesting equilibration of fabrics at high temperatures during or possibly after deformation, (3) garnets equilibrated at 700°–800°C, and associated aureoles and veins, commonly overprint the gneissic banding. The quartz-rich aureoles, as noted by *Compton* [1960], are generally equidimensional about the garnets, suggesting growth under isobaric postdeformational pressures. Together the above observations suggest that the gneissic banding of the Coast Ridge Belt is primarily a high-

Table 5. Sm-Nd Isotope Data for Minerals and Whole-Rock, Sample 710-5, Cone Peak

Sample	Sm, ppm	Nd, ppm	$^{147}Sm/^{144}Nd$[a]	$^{143}Nd/^{144}Nd$ (2σ)[b]
Plagioclase	0.979	6.260	0.0945	0.512612 ± 14
Biotite	5.000	19.815	0.1525	0.512639 ± 8
Amphibole	11.398	36.304	0.1898	0.512651 ± 9
Garnet-1	6.485	7.844	0.4998	0.512812 ± 11
Garnet-2	7.122	7.553	0.5702	0.512850 ± 15
Whole-rock	6.259	26.556	0.1425	0.512634 ± 7

[a]Parent-daughter ratios are precise to ~0.4%.
[b]$^{143}Nd/^{144}Nd$ normalized to $^{146}Nd/^{144}Nd = 0.7219$. Errors refer to the last two digits. Replicate analyses of La Jolla Nd standard measured during the course of this study yielded $^{143}Nd/^{144}Nd = 0.511852 \pm 8$.

temperature or subsolidus deformation feature, an axial planar foliation developed on isoclinal folds.

8. Interpretation

8.1. Age and Provenance of the Sur Series

[37] The original tectonic location of Salinia and the age and origin of its metasedimentary framework has been the subject of much speculation (see *Mattinson* [1990] for a summary). The debate has centered on whether Salinia is a far traveled terrane as suggested by some paleomagnetic data [e.g., *Kanter and Debiche*, 1985], or whether it has undergone only limited northward transport from an original location in the southern California arc [e.g., *Dickinson and Butler*, 1998]. The debate has not benefited from evidence relating to the depositional age of the Salinian metasedimentary framework, as medium-grade to high-grade metamorphism has precluded fossil preservation.

[38] We use the inherited zircon ages in the Cone Peak intrusion (Table 4, Figure 11) to constrain the origin of the framework rocks in the study area. While the zircons may have been derived from multiple sources in deeper parts of the arc, we make the simple assumption that they were part of the original Salinian sedimentary framework. The distribution of inherited ages in the sample is shown in Figure 11 and does not match any of the relative age-probability curves for major North and Central America stratigraphic units [e.g., *Stewart et al.*, 2001]. We note however the predominance of Grenville ages and a group of Paleozoic ages. With the exception of the Devonian ages, the closest match for this distribution is a mix of the major Cordilleran miogeocline formations if dominated by the extensive Late Proterozoic-Cambrian Wood Canyon formation [*Stewart et al.*, 2001]. Preliminary Nd isotopic analyses of two quartzites from the Sur Series ($\varepsilon_{Nd} = -15$ to -17 (M. Ducea, unpublished data, 2002)) are within the range of the ε_{Nd} of the Middle Proterozoic to Cambrian section in the southern Great Basin [*Farmer and Ball*, 1997]. The nearest source of Devonian zircons is either northern California sources such as the Bowman Lake batholith in the Sierra City mélange [*Hanson et al.*, 1988; *Harding et al.*, 2000] or the terranes of southern Mexico [*Gillis et al.*, 2001; G. Gehrels, unpublished data, 2002]. Our interpretation then is that the Sur series metasedimentary component is a mix of miogeocline-derived detritus with a Paleozoic magmatic component. This suggests a late Paleozoic or Mesozoic depositional age for rocks. Given the overall similarity to the relative age probability distribution of the Wood Canyon formation, we speculate that this unit, which is very extensive in the Mojave region, is an important source. However, the preliminary single crystal zircon U/Pb geochronology data presented here cannot unambiguously distinguish between the various hypothesized sources of framework rocks within Salinia (Figure 11).

8.2. A Largely Igneous Origin for the Coast Ridge Belt Framework Gneiss

[39] The Sur Series metamorphic framework of the Coast Ridge Belt differs from the shallower metamorphic framework rocks of the Santa Lucia Mountains in an increased concentration of granofels, amphibolites and marble, a near absence of biotite schists and a generally less foliated and more massive appearance of outcrops [*Ross*, 1976]. Although framework rocks in both areas are thought to represent a predominantly metasedimentary sequence [e.g., *Ross*, 1977], the results of field and geochronologic work presented here suggests that the sedimentary component of the Coast Ridge Belt is subordinate to metaigneous rocks. These interpretations are also supported by major element data [*Ducea et al.*, 2003b] and isotopic work [*Kidder et al.*, 2001].

[40] The original designation as a sedimentary sequence by *Trask* [1926] was based primarily on the abundance of marble and quartzite in the generally layered gneiss, and on the overall absence of cross cutting relationships. The bulk composition of the gneiss is one of a calc-alkaline tonalite, with subordinate granodiorites, based on the modal composition of rocks examined in thin sections. The U/Pb zircon age of the most deformed gneiss in the area is 93 Ma with no inheritance, which corresponds to a period of intense magmatism (''flare up'') in the California arc [*Ducea*, 2001, and references therein]. Gneissic rocks with the typical composition of the Sur Series are seen cross cutting the marble layers via tubes and dikes, suggesting intrusive relationships.

[41] *Kidder et al.* [2001] determined Sr and Nd isotopic ratios on five typical felsic and mafic samples of the Coast Ridge Belt gneiss and found them to be isotopically indistinguishable from the intrusive rocks in the section. For comparison, three less common framework rocks were also analyzed, including a quartzite, a quartzofeldspathic vein, and a quartzofeldspathic inclusion in a marble. All three were found to have significantly more evolved or ''metasedimentary'' isotope ratios than the gneisses. The 93 Ma U-Pb age presented here on a separate sample of the gneiss and the 81 Ma age on the gneiss exposed at Cone Peak clearly indicate Cordilleran magmatic origins for these rocks as well.

[42] We interpret therefore that the gneissic framework in the study area is predominantly metaigneous, arc-related, and that framework rocks of sedimentary origin are subordinate and generally limited to quartzites and marbles.

8.3. Igneous and Metamorphic History of the Coast Ridge Belt

[43] U-Pb data presented here provide a link between magmatic activity in the shallow level exposures dated throughout Salinia and the deeper crustal exposures studied here. The first evidence of Mesozoic igneous activity in the Coast Ridge Belt comes from a few inherited zircons of age $\sim$120 Ma found in two of the three analyzed samples (Table 4). Although no plutons of that age have been documented in the Coast Ridge Belt, this suggests that at least some magmatic activity had begun by that time. A pyroxene tonalite near Big Sur crystallized at 104 Ma [*Mattinson*, 1978] and is the next known magmatic event in the Coast Ridge Belt. Within the study area, three bodies intruded within a fairly short period of time in the late Cretaceous: a 93 Ma body now incorporated into the

framework gneiss, an 86 Ma diorite and an 81 Ma quartz diorite. Magmatic ages recorded with U-Pb and whole-rock Rb-Sr geochronology [*Kistler and Champion*, 2001] on shallower rocks throughout the Santa Lucia Mountains are also focused in the latest Cretaceous. Thus magmatic activity in the Santa Lucia Mountains apparently began with a few sporadic early and middle Cretaceous intrusions followed by a pulse of activity in the late Cretaceous. This pulse of magmatism may have corresponded with an eastward migration of magmatism across the Salinian arc [*Mattinson*, 1990].

[44] The accumulation of magmas in the Coast Ridge Belt led to a significant thickening of the section during the Late Cretaceous. Recognizable igneous bodies make up ~30% of the section and as mentioned above, much of the gneiss is Cretaceous orthogneiss. On the basis of whole rock geochemistry, our best estimate is that a conservative 60% and probably closer to 80% of the section is igneous or metaigneous [*Ducea et al.*, 2003b]. Thus, barring significant removal of material, the Coast Ridge Belt appears to have more than doubled in thickness between 93 and 80 Ma. These intrusions were split fairly evenly between felsic and mafic magmas, contrasting with the overwhelmingly felsic nature of contributions to the upper 20 km of the Salinian crust (>90% by volume). This distribution is presumably the result of magma stalling at levels of neutral density [*Glazner*, 1994].

[45] Peak recorded pressures and temperatures of 0.75 GPa and 800°C occurred throughout the section at the conclusion of this period, between 81 and 76 Ma, coinciding with the growth of postkinematic garnets and at least in part postdating igneous activity. Although there is no reported pressure-temperature evidence for magma loading in the region, the thickening we record in the middle crustal section combined with voluminous intrusion seen in the upper crust are consistent with overall crustal thickening in the Late Cretaceous.

8.4. Timing of Deformation and the Development of Foliation

[46] Magmatic activity from 93 to 81 Ma also corresponded with a period of high-temperature deformation in the middle crust. While deformation may have begun somewhat earlier or later than 93 Ma, this age on a strongly deformed outcrop of amalgamated 93 Ma igneous rocks and marble in the same section as much less deformed 86 and 81 Ma igneous bodies shows that extensive deformation occurred during this time period. High-temperature deformation ceased shortly after 81 Ma, as evidenced by the presence of euhedral 76 Ma garnets grown over foliation planes in the 81 Ma Cone Peak intrusion. We therefore suggest that the ductile deformation responsible for the development of the gneissic banding in the rocks took place between 93 and 76 Ma, synchronous with magmatism in the area.

[47] Foliation of the Coast Ridge Belt dips on average 30 degrees to the NE, and we suggest that this foliation was originally near horizontal, since the simplest explanation for overall northeastward decreasing regional metamorphic grade in the Santa Lucia mountains is a simple tilting of the original crustal column. A crude 30 degree ''untilting'' restores foliation in the Coast Ridge Belt to horizontal and brings barometric estimates into rough agreement with their depth in a restored Salinian Arc. The same ''untilting'' also helps to restore overall northeast dipping metasedimentary layers in the central Santa Lucia Range to horizontal [*Wiebe*, 1970a].

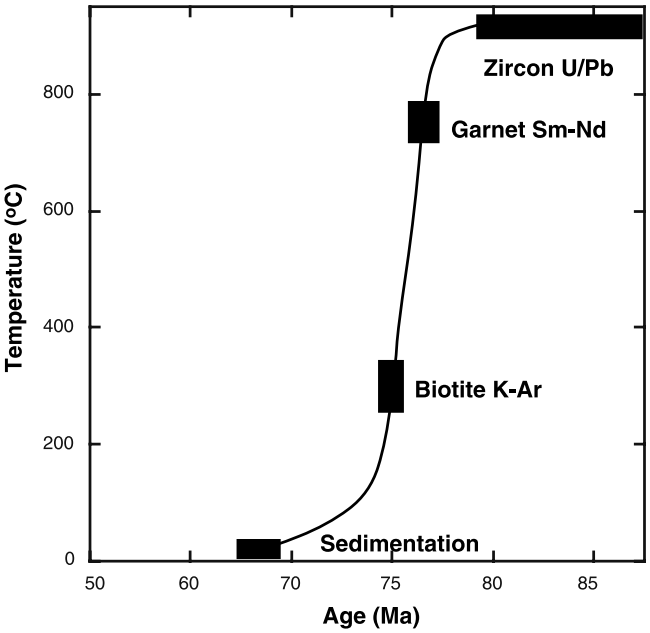

Figure 13. Diagrammatic plot of thermal histories for rocks near Cone Peak. See the text for details.

[48] Whether or not a correction for tilt is made, the metamorphic framework in the shallower exposures of the Santa Lucia Mountains to the east of the Coastal Ridge Belt differ in a few important ways from those in the Coast Ridge Belt itself. First, the shallower exposures have a generally steeper foliation. A second important distinction between the two areas is the contrast between the overall more uniform and layered appearance of the deeper rocks versus a more disorganized collection of plutons separating generally steeply dipping framework rocks in the shallower exposures. These differences in appearance may be explained if the middle crustal Coast Ridge Belt exposures represent a destination zone of supracrustal rocks displaced by granitic intrusions into the upper crust. The shallower and more steeply dipping rocks of the shallower exposures in this case represent ''metamorphic screens'' arrested in movement toward midcrustal levels. Similar upper crustal rocks were described by *Saleeby and Busby* [1993] in the Sierra Nevada batholith. This scenario hypothesizes an essentially ''pure shear'' environment for the Coast Ridge Belt consistent with the lack of consistent shear sense indicators associated with the high-temperature fabrics.

[49] An alternative explanation is that the fabric formed during ductile shearing of tectonic significance. It has been proposed [e.g., *Brown and Solar*, 1998] that intrusion of granitic bodies can take place along crustal-scale shear zones, and magmatism here is certainly associated with synchronous ductile deformation. In southern California, *May* [1989]

proposed that significant westward thrusting of the eastern Mojave arc took place between 90 and 80 Ma, as evident from ductile thrusting of arc-related rocks in the San Gabriel and San Bernardino Mountains. The coincidence of the timing of ductile deformation in the Coast Ridge Belt and Mojave region may be important in understanding the development of the Cretaceous arc in California, especially if Salinia originated in southern California. However, the structures observed in the 25 km deep exposure of the Coast Ridge Belt are markedly different from the ones described from shallower exposures in southern California by *May* [1989].

[50] The two hypothesis (thrusting *vs*. local return flow) may only be distinguished by a detailed field investigation of the transition area from midcrustal levels to the shallow exposures in the central Santa Lucia Mountains. However, our limited field evidence for a pure shear mechanism of deformation in the Coast Ridge Belt, argue against ductile thrusting.

8.5. Exhumation History

[51] Several lines of evidence suggest that the Cone Peak section was quickly cooled and exhumed after the cessation of magmatic activity at ~81 Ma. Our data indicate that the section was at high pressure-temperature at 76.5 Ma (from combined garnet geochronology and thermobarometry). A 75 Ma K-Ar date [*Compton*, 1966b] and an apatite fission track age of 71 Ma [*Naeser and Ross*, 1976] both obtained in the Cone Peak area suggest fast cooling following peak metamorphism at 76 Ma. Mineral cooling ages by K-Ar, Ar-Ar, U/Pb and Rb-Sr techniques from everywhere within the Santa Lucia Mountains show similar results, falling everywhere in the narrow range from about 83 to 69 Ma [*Kistler and Champion*, 2001]. The section was exposed to the surface and covered in the latest Cretaceous by coarse-grained submarine sediments derived in an extensional environment from local basement rocks and volcanic rocks of the California magmatic arc [*Grove*, 1993]. Although originally considered late Campanian [*Compton*, 1966a; *Howell and Vedder*, 1978], subsequent investigations have shown that the oldest sediments are either mid-Maastrichtian or early late Maastrichtian [*Saul*, 1986; *Seiders*, 1986; *Sliter*, 1986]. We estimate the time of final exhumation of the Cone Peak section to be ~68 Ma, corresponding to early-late Maastrichtian. The Maastrichtian sediments are in most places unconformably overlying Salinian basement; in a few outcrops, they are in strike-slip fault contact [e.g., *Compton*, 1966a], but the age of faulting is probably late Cenozoic.

[52] A temperature-age plot honoring the thermochronology and thermobarometry data for the Cone Peak section is shown in Figure 13. The section was unroofed at an average rate of at least 2–3 mm/yr, which is an order of magnitude higher than unroofing rates calculated for the Sierra Nevada arc [*House et al.*, 2001]. Such high unroofing rates require tectonic denudation in an extensional environment, since the area did not represent a topographic high at the time and may even have been submerged for most of the latest Cretaceous [*Grove*, 1993]. A NNW-SSE direction of extension during this period is suggested by mineral lineations measured in the study area. Timing of this medium-temperature structure is well constrained to this period of time as we know (1) that the fabric postdates the 93–80 Ma high-temperature structures, and (2) that temperatures in the Coast Ridge Belt did not exceed the apatite fission track closure temperature (110°C) since the latest Cretaceous [*Naeser and Ross*, 1976; *Ducea et al.*, 2003a].

[53] Exhumation of the Coast Ridge Belt may have been related to late Cretaceous extensional collapse of the entire section of the arc at the latitude of the present day Mojave region [e.g., *Wood and Saleeby*, 1997]. Late Cretaceous extensional collapse of the arc in that region is commonly attributed to underthrusting of the forearc at depths as shallow as 30 km [e.g., *Malin et al.*, 1995]. In the Salinian composite terrane, the Sierra de Salinas schist is the local equivalent of the forearc-related Pelona/Orocopia/Rand schists found in the Mojave region [see, e.g., *Jacobson et al.*, 2000; *Schott and Johnson*, 1998; *Mattinson*, 1990]. The Sierra de Salinas schist was emplaced into the southern California crust to depths of 25–30 km by 80 Ma [*Mattinson*, 1990]. Recently proposed tectonic models suggest that the North American upper plate of this thrust system had collapsed gravitationally by the end of the Cretaceous leading to the development of normal faults, the exposure of core complexes, and a subdued topography [*Saleeby et al.*, 2003]. In contrast, the main parts of the Sierra Nevada and Peninsular Ranges batholith have been slowly unroofed to a present-day average of 5–7 km [*House et al.*, 2001; *Saleeby et al.*, 2003].

[54] If magmatic cessation and extensional collapse are linked to late Cretaceous forearc underthrusting in the Salinian belt, then the rocks of the Coast Ridge Belt are the deepest exposures exhumed to the surface during the latest Cretaceous and may therefore represent the exposures closest to the major structural ramp of the system. In this scenario the existence of mafic to intermediate intrusions with North American isotopic signatures [*Kidder et al.*, 2001] intruded as late as 81 Ma places a maximum age on the beginning of forearc underthrusting. The postkinematic growth of garnet through the section may then have been the result of isobaric cooling due to this thrusting event.

9. Discussion

[55] The data and interpretations above provide constraints for understanding the tectonic and magmatic mechanisms that operate in continental arcs. We discuss here the implications of our observations to deciphering: (1) magmatic pulses in the Cordillera, and (2) ductile deformation in arcs.

[56] 1. We show that much of the midcrustal magmatism that led to the development of the Coast Belt Ridge was late Cretaceous, corresponding to the major Cretaceous flare up recorded from shallower exposures of the California arc [e.g., *Ducea*, 2001]. We observe that at the paleodepths of ~25 km of the Coast Ridge Belt, mafic materials are far more common at the time of the California arc flare up than they are anywhere in the shallow exposures. The mafic sills

have been emplaced throughout the magmatic pulse but have rarely escaped into the shallower levels of the crust. This observation suggests that the current depth of exposure in the Coast Ridge Belt represented the neutral level of buoyancy for mafic arc magmas.

[57] 2. We infer that the rocks of the Coast Ridge Belt and continuing to the east represent a tilted exposure of a Cordilleran magmatic arc with exposure depths ranging from 25 km in the west to some 10 km in the east. No major displacement have been mapped within this section. This section thus provides a transition from shallow ''batholithic'' depths where metamorphic screens (''pendants'') are vertical, to the level at which the foliation of the framework was essentially horizontal. We propose that the transition took place at about 25 km beneath the arc in this case and this paleodepth represents the root of large-scale, batholith forming intrusions. The ductile deformation is, in our interpretation, the result of localized return ductile flow of upper crustal materials (metasedimentary rocks and arc-related metaplutonic and metavolcanic rocks) in response to the upwelling of larger plutons [e.g., *Paterson and Miller*, 1998].

[58] Taken together, these interpretations are used to propose here that the roots of the large volume (hundreds of km^3 or larger) felsic plutons mapped in the North American Cordilleran batholiths are represented by a midcrustal low-strength zone spreading out horizontally as gravity current [*Wernicke and Getty*, 1997]. This zone is the destination for both mafic magmas ascending from the mantle wedge and localized ductile flow of plutonic rocks and metamorphic screens from the upper crust [*Ducea et al.*, 2003b]. Therefore this weak and hot midcrustal domain separating large felsic plutons from a mafic lower crust could: (1) act as a mechanical detachment surface during synmagmatic or postmagmatic regional thrusting, extension or convective removal, (2) provide an efficient zone of magma mixing and mingling during arc magmatism.

10. Conclusions

[59] Detailed mapping, petrography, thermobarometry and geochronology of rocks from the Cone Peak area support the following conclusions relevant to the regional geology:

[60] 1. The metamorphic framework rocks are predominantly orthogneisses with only subordinate amounts of quartzite and carbonate metasedimentary assemblages;

[61] 2. Inherited zircon ages in the Cone Peak quartz diorite suggest a connection between the ''Sur Series'' and the Wood Canyon formation in southern California, and suggest a late Paleozoic or younger sedimentary age for the Sur Series;

[62] 3. Substantial ductile deformation of the framework took place between 93 and 81 Ma, concomitant with intrusion in the section; most of the section was built by magmatic additions during that period;

[63] 4. Peak metamorphic conditions (800° C and 0.75 GPa) were achieved immediately after the last intrusion in the section between 81 and 76 Ma;

[64] 5. NNW-SSE oriented mineral lineations and mylonitic fabrics were developed at medium temperatures in the late Campanian-Maastrichtian during exhumation of the section at a rate of at least 2–3 mm/yr.

[65] Magmatism in the Coast Belt Ridge took place within the short period of late Cretaceous flare up of the California arc, further substantiating the notion that magmatism in the North American Cordillera was highly episodic. We propose that the arc midcrust here represents a zone of flattening of downward flowing supercrustal rocks and their convergence and mixing with stalling mafic magmas, presumably due to neutral buoyancy.

[66] **Acknowledgments.** Supported by NSF grant EAR-0229470 from the Petrology-Geochemistry Program (Ducea). Fieldwork was partly supported by the University of Arizona Geostructure Program and a grant from Chevron. Beth Duschatko, Alisa Miller, Elisabeth Nadin and Ken Domanik are thanked for their help in the field and lab. A special thanks to John Smiley at the Landels-Hill Big Creek Reserve for their hospitality and assistance. We are thankful to Jason Saleeby and Bill Dickinson for their constant support, enthusiasm, and willingness to share their knowledge of Cordilleran geology. Constructive reviews by James Mattinson, editor Brian Wernicke, and an anonymous reviewer have significantly improved the quality of the manuscript.

References

Barth, A. P., and D. J. May, Mineralogy and pressure-temperature-time path of Cretaceous granulite gneisses, south-eastern San Gabriel Mountains, southern California, *J. Metamorph. Geol.*, *10*, 529–544, 1992.

Barton, M. D., Cretaceous magmatism, metamorphism, and metallogeny in the east-central Great Basin, *Geol. Soc. Am. Mem.*, *174*, 283–302, 1990.

Brown, M., and G. S. Solar, Granite ascent and emplacement during contractional deformation in convergent orogens, *J. Struct. Geol.*, *20*, 1365–1393, 1998.

Champion, D. E., D. G. Howell, and C. S. Gromme, Paleomagnetic and geologic data indicating 2500 km of northward displacement for the Salinian and related terranes, California, *J. Geophys. Res.*, *89*, 7736–7752, 1984.

Christensen, N. I., and W. D. Mooney, Seismic velocity structure and composition of the continental crust: A global view, *J. Geophys. Res.*, *100*, 9761–9788, 1995.

Coleman, D. S., and A. F. Glazner, The Sierra Crest magmatic event: Rapid formation of juvenile crust during the Late Cretaceous in California, in *Integrated Earth and Environmental Evolution of the Southwestern United States: The Clarence A. Hall, Jr. Volume*, edited by W. G. Ernst and C. A. Nelson, pp. 253–272, Bellwether, Columbia, Md., 1998.

Compton, R. R., Charnockitic rocks of Santa Lucia Range, California, *Am. J. Sci.*, *258*, 609–636, 1960.

Compton, R. R., Analyses of Pliocene-Pleistocene deformation and stresses in northern Santa Lucia Range, California, *Geol. Soc. Am. Bull.*, *77*, 1361–1379, 1966a.

Compton, R. R., Granitic and metamorphic rocks of the Salinian block, California Coast Ranges, *Bull. Calif. Div. Mines Geol.*, *90*, 277–287, 1966b.

Dickinson, W. R., Cretaceous sinistral strike slip along Nacimiento Fault in coastal California, *AAPG Bull.*, *67*, 624–645, 1983.

Dickinson, W. R., and R. F. Butler, Coastal and Baja California paleomagnetism reconsidered, *Geol. Soc. Am. Bull.*, *110*, 1268–1280, 1998.

Ducea, M., The California Arc: Thick granitic batholiths, eclogitic residues, lithospheric-scale thrusting, and magmatic flare-ups, *Geol. Soc. Am. Today*, *11*, 4–10, 2001.

Ducea, M. N., and J. B. Saleeby, Buoyancy sources for a large, unrooted mountain range, the Sierra Nevada, California: Evidence from xenolith thermobarometry, *J. Geophys. Res.*, *101*, 8229–8244, 1996.

Ducea, M., M. House, and S. Kidder, Late Cenozoic denudation, bedrock and surface uplift rates in the Santa Lucia Mountains, California, *Geology*, *31*, 139–142, 2003a.

Ducea, M. N., S. Kidder, and G. Zandt, Arc composition at mid-crustal depths: Insights from the Coast Ridge Belt, Santa Lucia Mountains, California, *Geophys. Res. Lett.*, *30*(13), 1703, doi:10.1029/2002GL016297, 2003b.

Ducea, M. N., J. Ganguly, E. Rosenberg, P. J. Patchett, W. Cheng, and C. Isachsen, Sm-Nd dating of spatially controlled domains of garnet single crystals: A new method of high temperature thermochronology, *Earth Planet. Sci. Lett.*, *213*, 31–42, 2003c.

Eckert, J. O., Jr., R. C. Newton, and O. J. Kleppa, The H of reaction and recalibration of garnet-pyroxene-plagioclase-quartz geobarometers in the CMAS system by solution calorimetry, *Am. Mineral.*, *76*, 148–160, 1991.

Ellis, D. J., and D. H. Green, An experimental study of the effect of Ca upon garnet-clinopyroxene Fe-Mg exchange equilibria, *Contrib. Mineral. Petrol.*, *71*, 13–22, 1979.

Farmer, G. L., and T. T. Ball, Sources of middle Proterozoic to early Cambrian siliciclastic sedimentary rocks in the Great Basin: A Nd isotope study, *Geol. Soc. Am. Bull.*, *109*, 1193–1205, 1997.

Ganguly, J., and M. Tirone, Diffusion closure temperature and age of a mineral with arbitrary extent of diffusion: Theoretical formulation and applications, *Earth Planet. Sci. Lett.*, *170*, 131–140, 1999.

Ganguly, J., W. Cheng, and M. Tirone, Thermodynamics of aluminosilicate garnet solid solution: New experimental data, an optimized model, and thermometry applications, *Contrib. Mineral. Petrol.*, *126*, 137–151, 1996.

Gehrels, G. E., Introduction to detrital zircon studies of Paleozoic and Triassic strata in western Nevada and northern California, *Spec. Pap. Geol. Soc. Am.*, *347*, 17 pp., 2000.

Gillis, R. J., G. E. Gehrels, A. Flores de Dios, and J. Ruiz, Paleogeographic implications of detrital zircons from the Oaxaca terrane of southern Mexico, *GSA Abstr. Prog.*, *33*(6), A-428, 2001.

Glazner, A. F., Foundering of mafic plutons and density stratification of continental crust, *Geology*, *22*, 435–438, 1994.

Graeber, F. M., and G. Asch, Three-dimensional models of *P* wave velocity and *P*-to-*S* velocity ratio in the southern central Andes by simultaneous inversion of local earthquake data, *J. Geophys. Res.*, *104*, 20,237–20,256, 1999.

Grove, K., Latest Cretaceous basin formation within the Salinian Terrane of west-central California, *Geol. Soc. Am. Bull.*, *105*, 447–463, 1993.

Hall, C. A., Jr., Geology of the Point Sur-Lopez Point region, Coast Ranges, California: A part of the southern California Allochthon, *Spec. Pap. Geol. Soc. Am.*, *266*, 40 pp., 1991.

Hamilton, W. B., Tectonic setting and variations with depth of some Cretaceous and Cenozoic structural and magmatic systems of the Western United States, in *Metamorphism and Crustal Evolution of the Western United States*, *Rubey Ser.*, vol. 7, edited by W. G. Ernst, pp. 1–40, Prentice-Hall, Old Tappan, N. J., 1988.

Hansen, E., and M. Stuk, Orthopyroxene-bearing, mafic migmatites at Cone Peak, California: Evidence for the formation of migmatitic granulites by anatexis in an open system, *J. Metamorph. Geol.*, *11*, 291–307, 1993.

Hanson, R. E., J. B. Saleeby, and R. A. Schweickert, Composite Devonian island-arc batholith in the northern Sierra Nevada, California, *Geol. Soc. Am. Bull.*, *100*, 446–457, 1988.

Harding, J. P., G. E. Gehrels, D. S. Harwood, and G. H. Girty, Detrital zircon geochronology of the Shoo Fly Complex, northern Sierra terrane, northeastern California, *Spec. Pap. Geol. Soc. Am.*, *347*, 43–56, 2000.

Hill, M. L., and T. W. Dibblee Jr., San Andreas, Garlock, and Big Pine faults, California: A study of the character, history, and tectonic significance of their displacements, *Geol. Soc. Am. Bull.*, *64*, 443–458, 1953.

Hirth, G., and J. Tullis, Dislocation creep regimes in quartz aggregates, *J. Struct. Geol.*, *14*, 145–159, 1992.

House, M. A., B. P. Wernicke, and K. A. Farley, Paleogeomorphology of the Sierra Nevada, California, from (U-Th)/He ages in apatite, *Am. J. Sci.*, *301*, 77–102, 2001.

Howell, D. G., and J. G. Vedder, Late Cretaceous paleogeography of the Salinian Block, California, in *Mesozoic Paleogeography of the Western United States/Pacific Coast Paleogeography Symposium 2, April 26, 1978*, edited by D. G. Howell and K. A. McDougall, pp. 523–534, Pac. Sect. Soc. of Econ. Paleontol. and Mineral., Los Angeles, Calif., 1978.

Jacobson, C. E., A. P. Barth, and M. Grove, Late Cretaceous protolith age and provenanance of the Pelona and Orocopia schists, southern California: Implications for evolution of the Cordilleran margin, *Geology*, *28*, 219–222, 2000.

James, E. W., and J. M. Mattinson, Metamorphic history of the Salinian Block: An isotopic reconnaissance, in *Metamorphism and Crustal Evolution of the Western United States, Rubey Ser.*, vol. 7, edited by W. G. Ernst, pp. 938–952, Prentice-Hall, Old Tappan, N. J., 1988.

Jenning, C. W., and R. G. Strand, Geologic map of California, Olaf P. Jenkins ed., *Map*, Santa Cruz sheet, Calif., Div. of Mines and Geol., Sacramento, Calif., 1959.

Kanter, L. R., and M. Debiche, Modeling the motion histories of the Point Arena and central Salinian terranes, in *Tectonostratigraphic Terranes of the Circum-Pacific Region, Earth Sci. Ser.*, vol. 1, edited by D. Howell, pp. 227–238, Circum-Pac. Coun. for Energy and Mineral Res., Houston, Tex., 1985.

Kidder, S., M. N. Ducea, G. G. Gehrles, and B. Duschatko, A large range of Sr and Nd isotope ratios in a small deep-crustal exposure of a Cretaceous Cordilleran arc: Implications for arc magma evolution, *Eos Trans. AGU*, *82*(47), Fall Meet. Suppl., Abstract T41C-0884, 2001.

Kistler, R. W., and D. E. Champion, Rb-Sr whole-rock and mineral ages, K-Ar, (super 40) Ar/(super 39) Ar, and U-Pb mineral ages, and strontium, lead, neodymium, and oxygen isotopic compositions for granitic rocks from the salinian composite terrane, California, *U.S. Geol. Surv. Open File Rep., 01-453*, 83 pp., 2001.

Ludwig, K. J., Isoplot/Ex (rev. 2. 49), *Spec. Publ. 1a*, 56 pp., Berkeley Geochronol. Cent., Calif., 2001.

Malin, P. E., E. D. Goodman, T. L. Henyey, Y. G. Li, D. A. Okaya, and J. B. Saleeby, Significance of seismic reflections beneath a tilted exposure of deep continental crust, Tehachapi Mountains, California, *J. Geophys. Res.*, *100*, 2069–2087, 1995.

Mattinson, J. M., Age, origin, and thermal histories of some plutonic rocks from the Salinian Block of California, *Contrib. Mineral. Petrol.*, *67*, 233–245, 1978.

Mattinson, J. M., Petrogenesis and evolution of the Salinian magmatic arc, *Geol. Soc. Am. Mem.*, *174*, 237–250, 1990.

May, D. J., Late Cretaceous intra-arc thrusting in southern California, *Tectonics*, *8*, 1159–1173, 1989.

Naeser, C. W., and D. C. Ross, Fission-track ages of sphene and apatite of granitic rocks of the Salinian Block, Coast Ranges, California, *J. Res. U.S. Geol. Surv.*, *4*, 415–420, 1976.

Newton, R. C., and D. Perkins III, Thermodynamic calibration of geobarometers based on the assemblages garnet-plagioclase-orthopyroxene (clinopyroxene)-quartz, *Am. Mineral.*, *67*, 203–222, 1982.

Page, B. M., The southern Coast Ranges, in *The Geotectonic Development of California, Rubey Ser.*, vol. 1, edited by W. G. Ernst, pp. 329–417, Prentice-Hall, Old Tappan, N. J., 1981.

Passchier, C. W., and R. A. J. Trouw, *Microtectonics*, Springer-Verlag, New York, 1998.

Patchett, P. J., and J. Ruiz, Nd isotopic ages of crust formation and metamorphism in the Precambrian of eastern and southern Mexico, *Contrib. Mineral. Petrol.*, *96*, 523–528, 1987.

Paterson, S. R., and R. B. Miller, Mid-crustal magmatic sheets in the Cascades Mountains, Washington: Implications for magma ascent, *J. Struct. Geol.*, *20*, 1345–1363, 1998.

Pickett, D. A., and J. B. Saleeby, Thermobarometric constraints on the depth of exposure and conditions of plutonism and metamorphism at deep levels of the Sierra Nevada batholith, Tehachapi Mountains, California, *J. Geophys. Res.*, *98*, 609–629, 1993.

Powell, R. E., Balanced palinspastic reconstruction of pre-late Cenozoic paleogeology, southern California: Geologic and kinematic constraints on evolution of the San Andreas fault system, *Geol. Soc. Am. Mem.*, *178*, 1–106, 1993.

Pupin, J. P., Typologie des zircons des termes satures intermediaries et differencies des series alkalines du Mont-Dore et de la Chain de Puys (Massif Central Francais), *C. R. Acad. Sci., Ser. II*, *296*, 761–764, 1983.

Reich, P., Geology of the Lucia Quadrangle, California, *Calif. Univ. Publ. Geol. Sci. Bull.*, *24*, 115–168, 1937.

Ross, D. C., Reconnaissance geologic map of pre-Cenozoic basement rocks, northern Santa Lucia Range, Monterey County, *Map MF-750*, U.S. Geol. Surv., Reston, Va., 1976.

Ross, D. C., Pre-intrusive metasedimentary rocks of the Salinian block, California: A paleotectonic dilemma, in *Paleozoic Paleogeography of the Western United States: Pacific Coast Paleogeography Symposium I, April 22, 1977*, edited by J. H. Stewart, C. H. Stevens, and A. E. Fritsche, pp. 371–380, Pac. Sect. Soc. of Econ. Paleontol. and Mineral., Los Angeles, Calif., 1977.

Ross, D. C., The Salinian Block: A Mesozoic granitic orphan in the California Coast Ranges, in *Mesozoic Paleogeography of the Western United States: Pacific Coast Paleogeography Symposium 2, April 26, 1978*, edited by D. G. Howell and K. A. McDougall, pp. 509–522, Pac. Set. Soc. Of Econ. Paleontol. And Mineral., Los Angeles, Calif., 1978.

Ross, D. C., Possible correlations of basement rocks across the San Andreas, San Gregorio-Hosgri, and Rinconada-Reliz-King City faults, California, *U.S. Geol. Surv. Prof. Pap.*, *1317*, 37 pp., 1984.

Rudnick, R. L., Making continental crust, *Nature*, *378*, 571–578, 1995.

Rudnick, R. L., and D. M. Fountain, Nature and composition of the continental crust: A lower crustal perspective, *Rev. Geophys.*, *33*, 267–309, 1995.

Saleeby, J. B., and C. Busby, Paleogeographic and tectonic setting of axial and western metamorphic framework rocks of the southern Sierra Nevada, California, in *Mesozoic Paleogeography of the Western United States: II., Field Trip Guideb.*, vol. 71, edited by G. C. Dunne and K. A. K. A. McDougall, pp. 509–522, Pac. Sect. Soc. of Econ. Paleontol. and Mineral., Los Angeles, Calif., 1978.

Saleeby, J., M. Ducea, and D. Clemens-Knott, Production and loss of high-density batholithic root, southern Sierra Nevada, California, *Tectonics*, *22*, doi:10.1029/2002TC001374, 2003.

Saul, L. R., Mollusks of latest Cretaceous and Paleocene age, Lake Nacimiento, California, in *Geology of Upper Cretaceous and Lower Tertiary Rocks Near Lake Nacimiento, California., Field Trip Guideb.*, vol. 49, edited by K. Grove and S. Graham, pp. 25–31, Pac. Sect. Soc. of Econ. Paleontol. and Mineral., Los Angeles, Calif., 1986.

Schott, R. C., and C. M. Johnson, Sedimentary record of the Late Cretaceous thrusting and collapse of the Salinia-Mojave magmatic arc, *Geology*, *26*, 327–330, 1998.

Seiders, V. M., Structural geology of Upper Cretaceous and lower Tertiary rocks near the Nacimiento Fault, northwest of Lake Nacimiento, California, in *Geology of Upper Cretaceous and Lower Tertiary Rocks Near Lake Nacimiento, California., Field Trip Guideb.*, vol. 49, edited by K. Grove and S. Graham,

pp. 33–39, Pac. Sect. Soc. of Econ. Paleontol. and Mineral., Los Angeles, Calif., 1986.

Seiders, V. M., J. M. Joyce, K. A. Leverett, and H. McLean, Geologic map of part of the Ventana wilderness and the Black Butte, Bear Mountain, and Bear Canyon road less areas, Monterey County, California, *Map MF-1559-B*, U.S. Geol. Surv., Reston, Va., 1983.

Silver, L. T., and J. M. Mattinson, "Orphan Salinia" has a home (abstract), *Eos Trans. AGU*, *67*(44), 1215, 1986.

Sliter, W. V., Maastrichtian foraminifers from near Lake Nacimiento, California: Their paleoenvironmental interpretation and regional correlation, in *Geology of Upper Cretaceous and Lower Tertiary Rocks Near Lake Nacimiento, California., Field Trip Guideb.*, vol. 49, edited by K. Grove and S. Graham, pp. 17–24, Pac. Sect. Soc. of Econ., Paleontol. and Mineral., Los Angeles, Calif., 1986.

Smithson, S. B., R. A. Johnson, and Y. K. Wong, Mean crustal velocity: A critical parameter for interpreting crustal structure and crustal growth, *Earth Planet. Sci. Lett.*, *53*, 323–332, 1981.

Stacey, J. S., and J. D. Kramers, Approximation of terrestrial lead isotope evolution by a two-stage model, *Earth Planet. Sci. Lett.*, *26*, 207–221, 1975.

Stewart, J. H., G. E. Gehrels, A. P. Barth, P. K. Link, B. N. Christie, and C. T. Wrucke, Detrital zircon provenance of Mesoproterozoic to Cambrian arenites in the Western United States and northwestern Mexico, *Geol. Soc. Am. Bull.*, *113*, 1343–1356, 2001.

Trask, P. D., Geology of the Point Sur quadrangle, California, *Calif. Univ. Publ. Geol. Sci. Bull.*, *16*, 119–186, 1926.

Vedder, J. G., D. G. Howell, and H. McLean, Stratigraphy, sedimentation, and tectonic accretion of exotic terranes, southern Coast Ranges, California, *AAPG Memoir*, *34*, 471–496, 1982.

Wernicke, B. P., and S. R. Getty, Intracrustal subduction and gravity currents in the deep crust: Sm-Nd, Ar-Ar, and thermobarometric constraints from the Skagit Gneiss complex, Washington, *Geol. Soc. Am. Bull.*, *109*, 1149–1166, 1997.

Wiebe, R. A., Relations of granitic and gabbroic rocks, northern Santa Lucia range, California, *Geol. Soc. Am. Bull.*, *81*, 105–115, 1970a.

Wiebe, R. A., Pre-Cenozoic tectonic history of the Salinian block, western California, *Geol. Soc. Am. Bull.*, *81*, 1837–1842, 1970b.

Wood, D. J., and J. B. Saleeby, Late Cretaceous-Paleocene extensional collapse and disaggregation of the southernmost Sierra Nevada Batholith, *Int. Geol. Rev.*, *39*, 973–1009, 1997.

M. Ducea, G. Gehrels, S. Kidder, P. J. Patchett, and J. Vervoort, Department of Geosciences, University of Arizona, Gould-Simpson Building, 1040 East 4th Street, Tucson, AZ 85721-0077, USA. (ducea@geo.arizona.edu; ggehrels@geo.arizona.edu; skidder@geo.arizona.edu; patchett@geo.arizona.edu; vervoort@wsu.edu)